



저작자표시-비영리-변경금지 2.0 대한민국

이용자는 아래의 조건을 따르는 경우에 한하여 자유롭게

- 이 저작물을 복제, 배포, 전송, 전시, 공연 및 방송할 수 있습니다.

다음과 같은 조건을 따라야 합니다:



저작자표시. 귀하는 원저작자를 표시하여야 합니다.



비영리. 귀하는 이 저작물을 영리 목적으로 이용할 수 없습니다.



변경금지. 귀하는 이 저작물을 개작, 변형 또는 가공할 수 없습니다.

- 귀하는, 이 저작물의 재이용이나 배포의 경우, 이 저작물에 적용된 이용허락조건을 명확하게 나타내어야 합니다.
- 저작권자로부터 별도의 허가를 받으면 이러한 조건들은 적용되지 않습니다.

저작권법에 따른 이용자의 권리는 위의 내용에 의하여 영향을 받지 않습니다.

이것은 [이용허락규약\(Legal Code\)](#)을 이해하기 쉽게 요약한 것입니다.

[Disclaimer](#)

Master's Thesis

Finite element model of the drilling process of  
carbon fiber reinforced plastic (CFRP)

Min Ji Kim

Department of Mechanical Engineering

Graduate school of UNIST

2017

# Finite element model of the drilling process of carbon fiber reinforced plastic (CFRP)

Min Ji Kim

Department of Mechanical Engineering

Graduate School of UNIST

# Finite element model of the drilling process of carbon fiber reinforced plastic (CFRP)

A thesis  
submitted to the Graduate School of UNIST  
in partial fulfillment of the  
requirements for the degree of  
Master of Science

Min Ji Kim

06. 13. 2017

Approved by

---

Advisor  
Prof. Hyung Wook Park

# Finite element model of the drilling process of carbon fiber reinforced plastic (CFRP)

Min Ji Kim

This certifies that the thesis of Min Ji Kim is approved.

06. 13. 2017

signature

---

Thesis Supervisor: Prof. Hyung Wook Park

signature

---

Prof. Young-Bin Park

signature

---

Prof. NamHun Kim

## ABSTRACT

Carbon fiber reinforced plastic (CFRP) is a composite, composed of reinforcing carbon fiber and matrix resin. CFRP is widely used in various fields, such as aerospace, automotive, robotics, and civil infrastructures, due to its excellent corrosion resistance and superior physical characteristics like strength-to-weight ratio, compared with traditional metals. Therefore, it has been constantly utilized and developed as the state-of-the-art material in numerous applications. Machining is indispensable when applying CFRP in these various industries, among which drilling process is indispensable for assembling different parts into products. However, unlike metals, CFRP holds heterogeneous properties. During the drilling process, delamination and uncut fibers are generated by the thrust force generated in the feed direction. While delamination at the outer surface can be detected by visual inspection, internal defect cannot be observed by the naked eye. These defects need to be predicted because of not only reducing the durability of the product but also causing deterioration in quality.

This thesis presents the simplified FE model and method to predict the mechanical phenomena during the drilling process. To investigate these phenomena, a simulation model was developed with commercial FEM software, ABAQUS. Through the developed FE model, it was possible to predict the delamination through the stress distribution of each layer generated after the drilling process. In addition, it was possible to identify uncut fibers for each layer through this, and furthermore, the possibility of suggesting optimum processing conditions can be confirmed. Also, based on the analysis data obtained from the FE model, the change in the thrust force according to the drill entry position at the time of drilling was confirmed, and the accuracy of the developed analytical model was confirmed by comparing the experimental data with the analytical data.

Therefore, FE model was developed to investigate defect prediction, and the results from FE analysis was compared this with experimental data to minimize errors in CFRP drilling process.



## CONTENTS

1. INTRODUCTION .....	1
1.1 Background .....	1
1.2 Research objectives and approach .....	2
1.3 Thesis organization .....	3
2. LITERATURE REVIEW .....	4
2.1 Cutting mechanism of Carbon Fiber Reinforced Plastic (CFRP) .....	4
2.1.1 Machining of composite materials .....	4
2.1.2 Chip formation in composite machining .....	5
2.2 Modeling of Carbon Fiber Reinforced Plastic (CFRP) drilling .....	9
2.2.1 Failure criteria .....	12
2.2.2 Cohesive zone model .....	14
2.2.3 Drilling modeling .....	16
2.3 Summary .....	19
3. CARBON FIBER REINFORCED PLASTIC DRILLING MODEL FOR PREDICTION OF DEFECTS .....	20
3.1 FE model setup .....	20
3.1.1 Geometry modeling .....	21
3.1.2 Boundary condition .....	22
3.1.3 Element and mesh types .....	23
3.2 Material property .....	24
3.3 Damage modeling .....	25
3.4 Delamination modeling .....	27
3.4.1 Contact and friction coefficient .....	29
3.5 Experimental setup .....	31
3.6 Summary .....	34
4. VERIFICATION OF FINITE ELEMENT MODEL AND EXPERIMENTAL RESULTS .....	35
4.1 FE model results of Carbon Fiber Reinforced Plastic (CFRP) drilling .....	35
4.1.1 Thrust force of FE model. ....	36
4.1.2 Stress contour of FE model. ....	37



4.2 Comparison of FE model and experimental results .....	39
4.2.1 Thrust force .....	39
4.2.2 Chip morphology.....	45
4.2.3 Defects.....	46
4.3 Summary .....	48
5. CONCLUSIONS AND FUTURE WORK .....	49
5.1 Contributions and Conclusions .....	49
5.2 Future work .....	50

## LIST OF FIGURE

Fig. 1-1. Flow chart of thesis organization. ....	3
Fig. 2-1. The definition of the cutting variable .....	5
Fig. 2-2. Schematic view of different fiber angle orientations .....	6
Fig. 2-3. Chip formation mode for 0° fiber orientation cutting with positive rake angle .....	7
Fig. 2-4. Chip formation mode for 0° fiber orientation cutting with negative rake angle .....	7
Fig. 2-5. Chip formation mode for 45° fiber orientation (a) positive rake angle (b) negative rake angle.....	7
Fig. 2-6. Chip formation mode for 90° fiber orientation .....	8
Fig. 2-7. Chip formation mode for 135° fiber orientation .....	9
Fig. 2-8. Principal aspects to be considered when drilling fiber reinforced plastics .....	10
Fig. 2-9. Calculated matrix damage distributions in the macroscopic model (left) and the microscopic model (right): top row for a fiber orientation of 90° and bottom row for 0° fiber orientation .....	11
Fig. 2-10. Simulation results for different fiber angles workpiece (a) 0° (b) 90° (c) 135°.....	15
Fig. 2-11. Finite-element model of drilling T300/LTM-45EL CFRP laminate. (For interpretation of the references to colour in this figure legend, the reader is referred to the web version of this article.) ...	16
Fig. 2-12. Section of the hole during penetration of the drill simulated with complete model: (a) entrance and (b) exit of the drill .....	17
Fig. 2-13. Scheme of the pre-drilled hole in the simplified model .....	17
Fig. 2-14. Scheme of the complete model. Drill entrance simulation: (a) initial and (b) final drill position .....	18
Fig. 2-15. Model of the geometries: helical new (a) helical honed (b) and step (c) .....	18
Fig. 3-1. Progress of Carbon Fiber Reinforced Plastic (CFRP) drilling simplification.....	20
Fig. 3-2. Simplicity of FE model geometry.....	22
Fig. 3-3. Boundary condition of the FE model. ....	22
Fig. 3-4. Mesh of FE model (a) fabric CFRP (b) drill (c) jig top and bottom .....	23
Fig. 3-5. Algorithm of VUMAT in ABAUS/explicit .....	25
Fig. 3-6. Damage initiation, criterion and evolution in the interface cohesive.....	28
Fig. 3-7. Friction test (pin-on-disc test) setup.....	29
Fig. 3-8. Friction test (a) fabric CFRP specimens of friction test (b) friction coefficient result.....	30
Fig. 3-9. Experimental setup for CFRP drilling.....	31
Fig. 3-10. (a) Drill bit (b) fabric CFRP specimen for CFRP drilling .....	32

Fig. 3-11. CFRP drilling experimental setup.....	32
Fig.3-12. Design drawing of fixture systems (a) drill bush (b) jig top (c) jig bottom .....	32
Fig. 4-1. Process to verify the FE model. ....	35
Fig. 4-2. Position of a drill bit under the drilling process.....	36
Fig. 4-3. Thrust force of CFRP drilling simulation.....	37
Fig. 4-4. Stress contour of FE model (a) 5000rpm (b) 6000rpm (c) 7000rpm .....	38
Fig. 4-5. Cutting force of X-direction (5000rpm, 0.06mm/rev) (a) experimental result (b) simulation result.....	40
Fig. 4-6. Cutting force of Y-direction (5000rpm, 0.06mm/rev) (a) experimental result (b) simulation result.....	41
Fig. 4-7. Thrust force of Z-direction (5000rpm, 0.06mm/rev) (a) experimental result (b) simulation result.....	42
Fig. 4-8. Thrust force comparison with FE model and experiment (a) 5000rpm (b) 6000rpm (c) 7000rpm.....	43
Fig. 4-9. Chip morphology (a) experimental chip (b) FE model chip. ....	45
Fig. 4-10. SEM image of CFRP chip morphology (a) fiber orientation $<90^\circ$ (b) fiber orientation $>90^\circ$ .....	46
Fig. 4-11. Defects comparison of FE model and experimental result after drilling process (5000rpm, 0.06mm/rev).....	47
Fig. 4-12. Comparison of CFRP specimens between FE model and experimental results .....	47

## **LIST OF TABLES**

Table 3-1. Machining parameters in fabric CFRP. ....	22
Table 3-2. Properties of fabric CFRP.....	24
Table 3-3. Strength properties of fabric CFRP. ....	27
Table 3-4. Material properties used in cohesive of the interface. ....	28
Table 3-5. Pin-on-disc test conditions. ....	30
Table 4-1. Thrust force of FE drilling model. ....	37
Table 4-2. Thrust force comparison of simulation and experiment.....	44

# 1. INTRODUCTION

## 1.1 Background

Carbon fiber reinforced plastic (CFRP) is a composite material constituted of reinforcing carbon fiber and polymer matrix. CFRP machining has several unique phenomena and characteristics compared to metal cutting. The main characteristic of metal machining is plastic deformation, but this is not valid in fiber reinforced plastic (FRP) machining. Plus, chip morphologies of CFRP cutting are observed as dust and abrasive chip in contrast to a chip flow over the tool edge during the metal machining.

CFRPs have various superior mechanical properties such as higher corrosive resistance, higher tensile strength-to-weight ratio, and lower weight to those of metals. Due to these advantages, CFRPs are utilized in numerous industries such as aerospace, aviation, and automotive. Among the wide applications, CFRP machining has become indispensable in aerospace and automotive, because the drilling process is compulsory for assembling adjacent parts.

In spite of many advantages of CFRP, there are some critical problems in terms of the drilling. During the drilling to a workpiece, there are unnecessary forces which lead to tool-life-reduction, delamination, poor surface quality, and hole size inaccuracy. The accuracy of the hole size is the important factor in drilling, and is affected by the forces induced from the drilling. There are damages in the workpiece, temperature increase, plasticity and friction between a drill and a workpiece. These problems are generated from the discrepancy between the FRP drilling and that of metal.

The main issues during CFRP drilling are delamination, tool wear and surface roughness. These defects can downgrade the material characteristics, and lower the mechanical properties. For example, it caused 60% of rejections in final step of the product assembly in the aerospace industry [1]. Therefore, it was imperative to find other drilling methods to minimize delamination [2-4]. There are some methods to decrease delamination based on proper cutting conditions, tool coating, tool geometry etc.

Thrust force and delamination in the drilling process is able to be predicted using analytical and numerical models. Analytical researches have predicted thrust force with the start of FRP delamination. Hocheng and Dharan developed the first analytical model [5]. This model showed that delamination can occur when thrust force exceeds the critical thrust force. After this proposal, other models have also been suggested [6-9]. Finite element models of CFRP are essential in the understanding and optimizing machining processes. The computational simulation analysis has been getting higher reliability and accuracy so that it is able to predict mechanical properties perfectly such as cutting force, stress distributions and so on. In this context, performing all drilling experiments is relatively irrational, in terms of economic and time-wasting issues. Therefore, finite element analysis (FEA) is required to simulate the FRP machining process with the aid of computer aided engineering (CAE) technology with

minimized or without experiments, considering the economic and temporal issues.

Many researchers investigated the correlations between thrust force and other elements during CFRP machining. Arula and Ramulu presented FEA which used maximum stress and Tsai-Hill criteria of orthogonal machining of composite [10]. Also, they have concluded that chip formation and material removal are correlated with fiber orientation. Other researchers presented 3D drilling FE model which simplified unidirectional CFRP orthogonal model [11, 12]. They developed the model using a fracture mechanism and virtual crack extension (VCE) method. Other studies have also been carried out regarding delamination and thrust force in composite drilling [13, 14]. In these researches, delamination modeling used a cohesive element in laminate interface. The model typically predicts the thrust force lower than the numerical models. However, none of the previous numerical researches have considered FE model according to the kind of the jig systems.

In this thesis, FE model of CFRP drilling was developed considering the jig system. The FE model takes account of a jig and a drill bush. All FE model applied the same cutting conditions and boundary conditions. The model consists of fabric carbon fiber plies stacked in different orientations. Therefore, this model can predict the intra-ply damage and delamination, which is inter-laminar debonding. To validate FE model, thrust force and machinability in relevant to the hole quality were investigated by CFRP drilling process. Furthermore, developed FE model was available to predict defects and it considered the feed rates and spindle speeds, and verified the model comparing the experimental results.

## 1.2 Research objectives and approach

The objectives of this study were to consist an FE model to simulate CFRP drilling. We performed the geometry simplification of the drill and CFRP specimen to build the FE model using commercial simulation tool by ABQUS. Next, we compared the results of CFRP drilling FE model and those of experimental. The main study aims were as follows:

- To verify accuracy of developed FE model of CFRP drilling process.
- To investigate the proper cutting condition during CFRP drilling process.
- To predict the defects such as delamination and uncut fiber investigated in CFRP specimen after CFRP drilling.

This study involved four stages:

Step 1: Investigate the characteristics of CFRP drilling.

Step 2: Carry out the experimental CFRP drilling.

Step 3: Perform the simulation of CFRP drilling with various spindle speeds and feed rates.

Step 4: Verify the coincidence between the results of the FE model and that of experimental by

comparing the thrust force, the stress contour, and picture.

### 1.3 Thesis organization

This thesis consisted in figure 1-2. Chapter 2 presents related literatures and studies in characteristics of CFRP machining, chip morphology, and CFRP drilling modeling. Chapter 3 describes the FE model setup and experimental setup for CFRP drilling. Chapter 4 compares the FE model with experimental results regarding thrust force and defects. Finally, Chapter 5 presents the conclusions of this study and future work for advanced work.

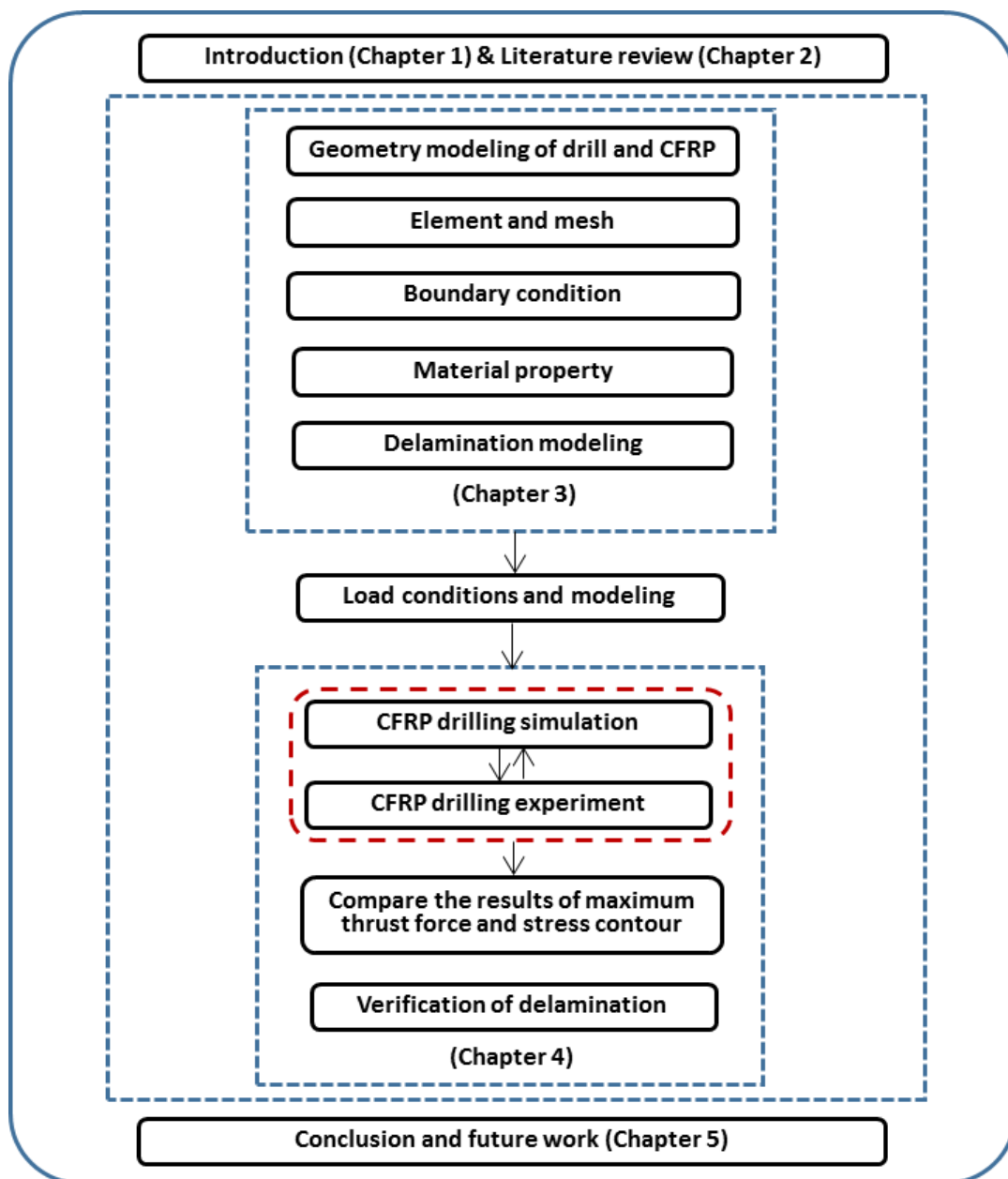


Fig. 1-1. Flow chart of thesis organization

## 2. LITERATURE REVIEW

This chapter shows a review of advanced research in involved with proposed works. Overview regarding past and current research relevant with CFRP drilling to predict the defects. Outline of the literature review consists of three contents; (1) Cutting mechanism of carbon fiber reinforced plastics (CFRPs) (2) Defects in CFRP drilling (3) Modeling of CFRP machining. Modeling of drilling system will involve the general researches regarding the dynamic behavior. The predictive FEM model will include the general theory of drilling and research of characteristic in CFRP machining. Review of the FEM for CFRP drilling will discuss FEM process applied for CFRP drilling system.

### 2.1 Cutting mechanism of carbon fiber reinforced plastic (CFRP)

Fiber reinforced plastics (FRPs) have different characteristics when they are machined in contrast with metal machining, due to the composite materials are anisotropic materials [15]. They are features such as stronger than steel and their high corrosion resistance. The most of metals are ductile and homogeneous, which are specified by elastics and plastic deformation, and occurrence of the continuous chip when they are machined. The results of the metal cutting process reach converging state which the cutting forces and surface conditions could be anticipated to the proper accuracy in opposition to the machining of the composite materials. Thrust force during machining of FRPs is fluctuating because of the fracture of the fibers. While the fibers are broken by the cutting edge, the fiber suffer from the shearing and bending by the advancing cutting edge during the composite machining. Therefore, the machining quality is affected by the fiber and its orientation [16]. The criteria measurement was more difficult for fiber reinforced plastics than that for metals due to the anisotropic and inhomogeneous structure. Delamination occurs by the low inter-laminate strength in the structure and high transverse forces depend on cutting.

#### 2.1.1 Machining of composite materials

The FRPs have machinability according to the mechanical properties of the composite and fiber orientation [17]. While carbon fibers are apt to be broken in brittle form by the cutting edge, the fiber tend to be bent in the cutting edge to escape the fiber shearing. Therefore, machined surface quality depends on the type of fiber strength and orientation, and the cutting conditions are rely on the fiber and the matrix strength. The chip morphology is influenced on the cutting condition, polymer type and tool geometry.

The polymer matrix in the FRPs is an important affectation in the chip formation and its types, since



its strength and stiffness are low-grader than those of reinforcement fibers, and they have at least resistance as the cutting. Moreover, the behavior of polymer cutting is influenced on cutting condition; tool materials, rake angle, cutting edge radius, depth of cut and cutting speed.

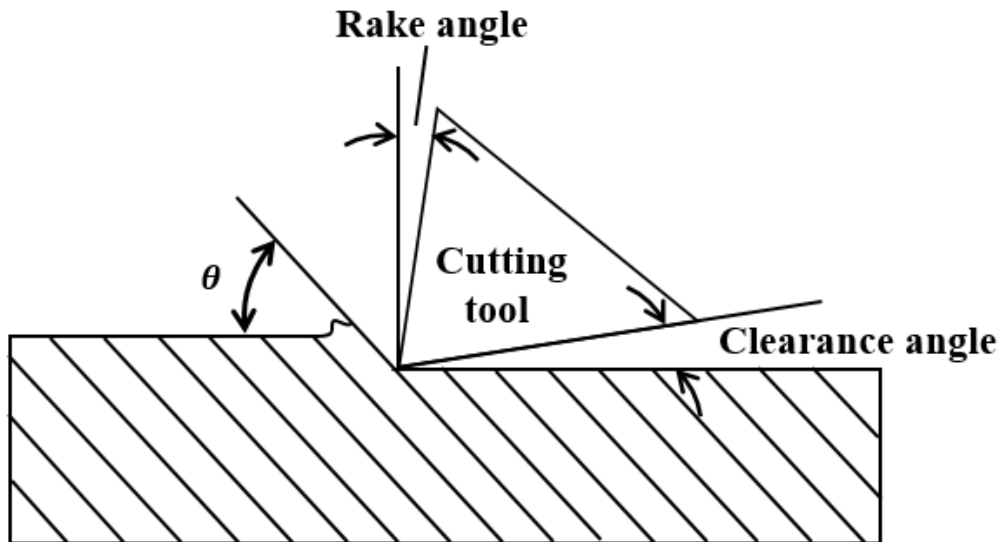


Fig. 2-1. The definition of the cutting variable [18]

Wang *et al.* [18] had been studied the orthogonal cutting of unidirectional FRPs, they discussed mechanisms (Fig. 1-1) of orthogonal cutting and chip formation regarding the fiber orientation, tool geometry, cutting condition and machinability. They used UD graphite/epoxy composite materials at various orientation using PCD tool. They aimed that the factor of the material deletion mechanisms is affectation with the fiber orientation. In the figure 1-1, the fiber orientation,  $\theta$ , determined clockwise. The cutting tools used a clearance angle of  $7^\circ$  and rake angles from  $20^\circ$  to  $40^\circ$ . They studied a unidirectional fiber arrangements larger than  $90^\circ$ .

### 2.1.2 Chip formation machining in composite machining

The machining of CFRP is different of the metal cutting in that the chip formation are used for the most of composite machining. There are several failure mechanisms in FRPs cutting different with the metal cutting. The failure mechanisms consist of the fiber failure, matrix failure, the layer delamination, matrix dent and separation between the fiber and the matrix in FRPs cutting. The five modes of FRPs chip formation are relevant to the polymer sort and the cutting conditions [19-27]. A continuous chip is made by cutting a ductile material, which is made from the plastic deformation, and is formed when thermoplastic matrix is cut. The chip morphology is alike with the chip machined the ductile metals. The discontinuous chip morphology is made when brittle materials are cut by large depth of cut. Since

the knowledge regarding FRPs cutting is limited, it is important to investigate the machining characteristics according to fiber orientation. The alteration of fiber orientation considering the cutting direction as shown in figure 2-2, and is an important factor in the definition of chip formation and machined surface during the FRPs material cutting.

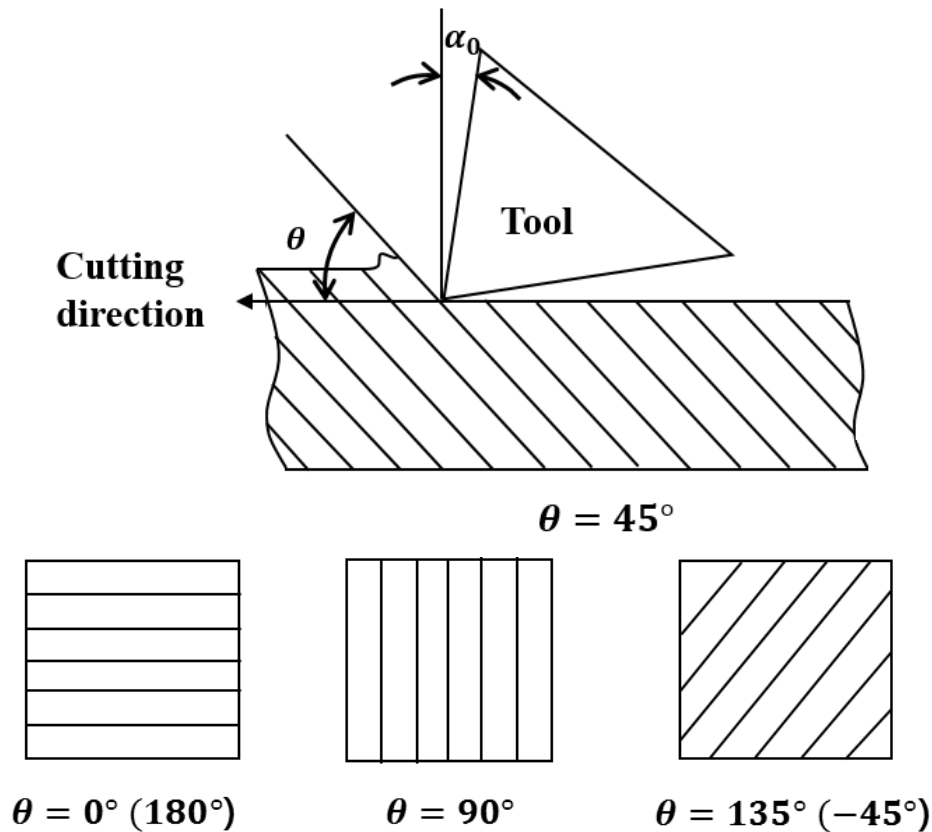


Fig. 2-2. Schematic view of different fiber angle orientations [19]

Unpredicted fracture is occurred by the CFRP machining that make with very little plastic deformation [19]. The chip formation mechanisms in the other researches when unidirectional FRPs have machining essentially considered that the fiber orientation and cutting edge have an effect the factors of the chip morphology. They can consist of 5 types [19, 21, 22].

First fracture type demonstrates delamination when the  $0^\circ$  fiber is cut. Delamination takes place when  $0^\circ$  fiber orientation cut with the tool of positive rake angle. The crack and propagation take place at the interface between an insert tool and FRPs. The bending moment by the failure occurs at the front of cutting edge as shown figure 2-3. The cutting force fluctuates such as upward-downward while the delamination-bending-fracture is repeated.

Second fracture type is generated by buckling when the  $0^\circ$  fiber is machined with negative rake angle tool. The buckling is induced by the compression along with the fiber direction and the direction of tool

movement. The progression of the tool bring about the results that make the fracture at the interface between the fiber and matrix, and the fiber is caused by the buckling. The results of the fracture are generated with the discontinuous chip such as the dust. The term of the fracture repeat is briefer than the fracture repeat of first fracture, therefore, the cutting force fluctuate smaller as shown in figure 2-4.

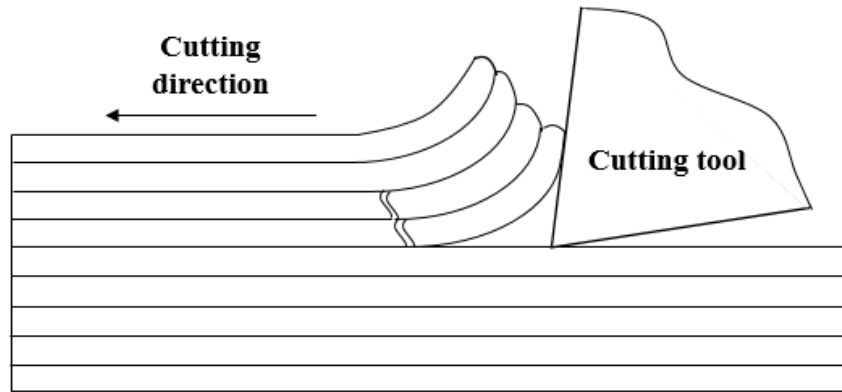


Fig. 2-3. Chip formation mode for  $0^\circ$  fiber orientation cutting with positive rake angle [19]

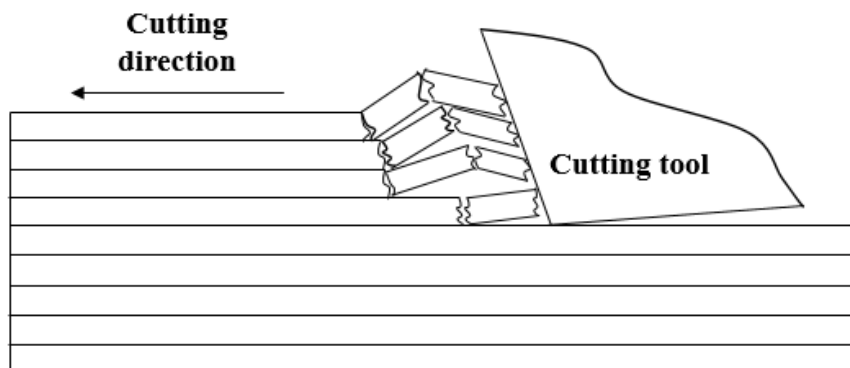
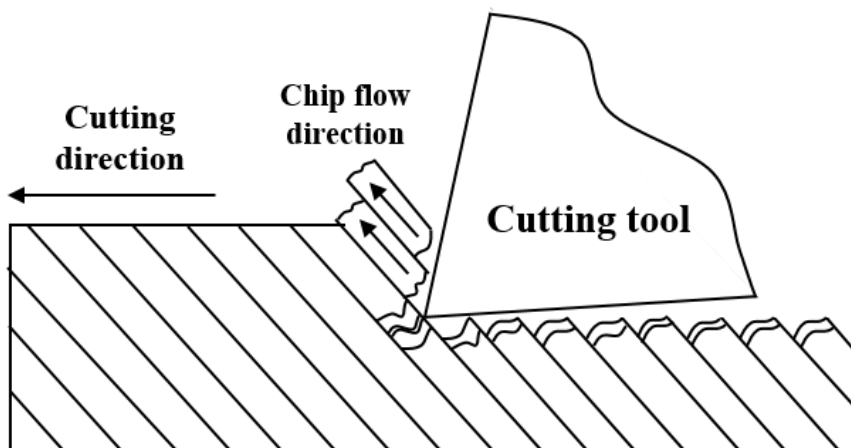


Fig. 2-4. Chip formation mode for  $0^\circ$  fiber orientation cutting with negative rake angle [19]



(a)

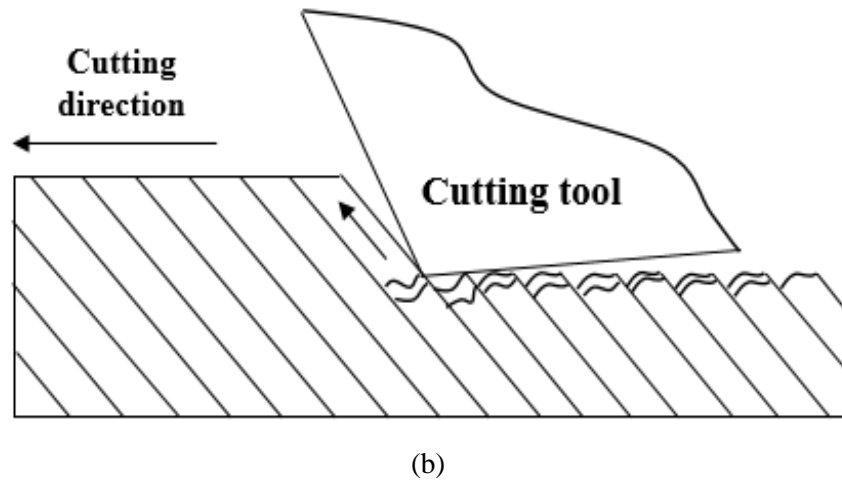


Fig. 2-5. Chip formation mode for 45° fiber orientation (a) positive rake angle (b) negative rake angle[19]

Third fracture mechanism is caused by fiber cutting during the FRP machining with the fiber orientation angle between 0° and 90° with the tool of positive and negative rake angle. The fracture is occurred by the compression along with the axis of the fiber when the fiber is cut. The interface fracture of laminate take places depending on the boundary between the fiber and the matrix during cutting process. The cracks in the fibers are occurred by the compression in up and down the cutting surface as shown in figure 2-5, and those phenomenon are able to find using the microscope. The chip flow direction is similar to the fiber orientation during machining with the tool of positive rake angle. The deformation of the metal is occurred by the plastic shear when metal is cut, but the plastic deformation is generated when FRPs is cut.

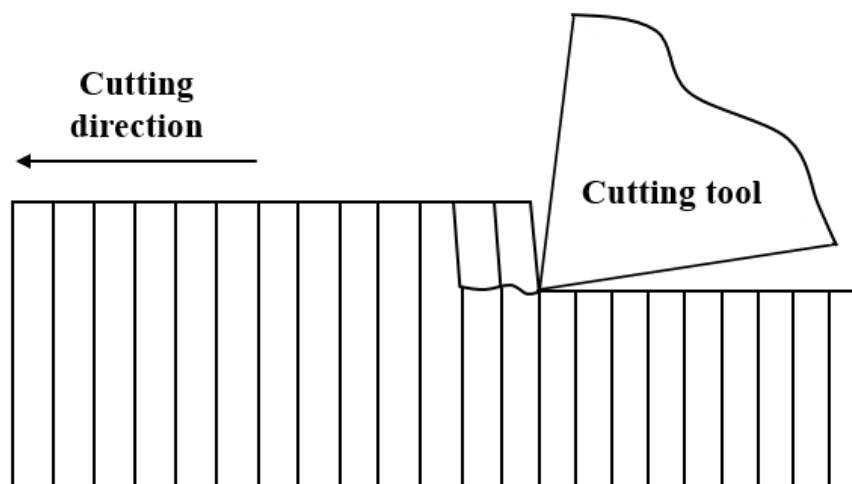


Fig. 2-6. Chip formation mode for 90° fiber orientation [19]

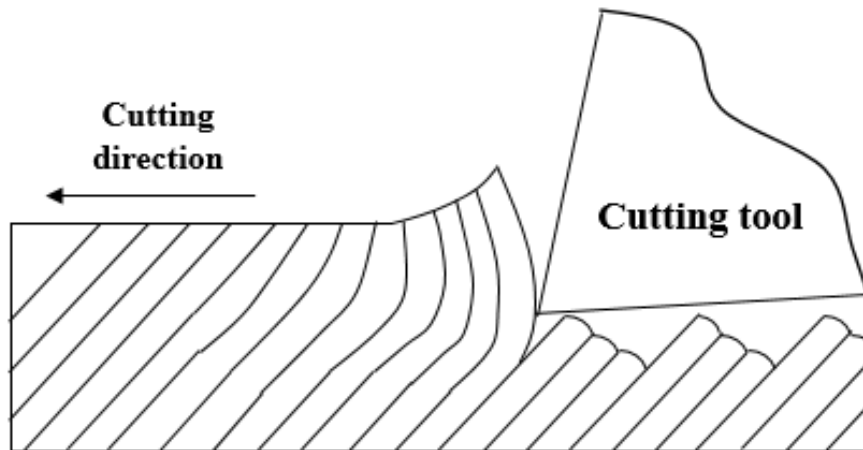


Fig. 2-7. Chip formation mode for 135° fiber orientation [19]

Fourth fracture type is caused by deformation in fiber orientation at  $\theta=90^\circ$ , which is obtained with a discontinuous chip.

Fifth fracture type is shearing, which generates when the fiber orientation is  $105^\circ < \theta < 150^\circ$  during the FRPs cutting. The fiber deformation is occurred by the compression forces, the result of that is generated to delamination in inter laminar along with the fiber-matrix interface. The fiber has elastic bending during the fiber cutting as shown in figure 2-7. In the results of this case, the tool edge is occurred with the crack in the fiber-matrix by the compressive stress, and the chip shape is a discontinuous long.

## 2.2 Modeling of the Carbon Fiber Reinforced Plastic (CFRP)

The experimental studies are expensive and time consuming, it is important to create the FEM modeling that can predict the output such as the defects and the characteristic of the machining. An FEM analysis presents the rough solutions to difficult problems. The results of an FEM analysis can aim of increasing the effectiveness in the cutting process [28, 29].

Drilling of FRPs can be considered a vital operation because to the tendency of delamination when undergone the mechanical stresses. The principal defects depend on delamination, pullout in exit site and improper surface roughness in the hole wall. Many kinds of defects occurred by drilling, delamination emerges to be the most critical. It is essential to select proper cutting conditions, due to the fact that the selection of inadequate condition could cause unreasonable results. The factors shown in figure 2-8 like cutting parameters and tool geometry/material must be considered aiming to obtain the optimal performance in drilling experiments, and best hole quality, which was state of minimum damage and satisfactory machined surface [15].

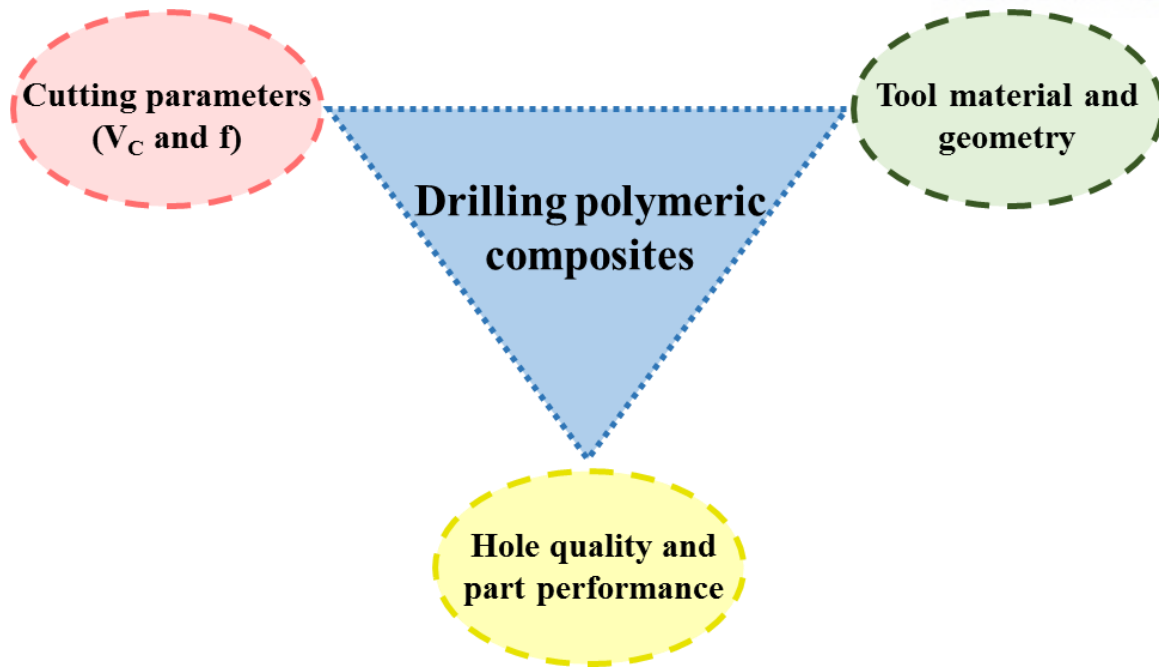


Fig. 2-8. Principal aspects to be considered when drilling fiber reinforced plastics [17].

Lasri *et al.* [30] developed 2-dimensional FE model to suggest the chip formation and damage initiation and propagation when UD-CFRP machining is progressed, and they investigated the effect of fiber orientation and overall failure process in UD-CFRP. This FEM model simulated the matrix cracking, debonding between fiber and matrix, and fiber failure. They observed the failure in around the tool edge and the damage propagation along with the fiber orientation, because the surface failure is influenced by the fiber orientation. The simulation results were different by the fiber orientation. The 30° fiber had small damage, and beyond the 45° fiber had increasing damage in the interface during the simulation. The debonding was occur between fiber and matrix when the cutting Unidirectional composite, following the matrix crashing and the fiber failure. They predicted the principal cutting force by the experimental operation from the literature. The thrust force was underestimated and that value was assumed to the repeatedly bounce back.

Venu Gopala *et al.* [31, 32] developed 2-dimensional Macro and micro FEM model that was used by ABAQUS. The model presented the orthogonal cutting of Unidirectional Glass Reinforced Polymer (UD GFRP) which consisted of the fiber and matrix separately in the FEM model. Fiber and matrix were modelled as equivalent orthotropic homogeneous material. To observe the phenomenon in the interface, they used the cohesive zone elements that were the zero thickness. They investigated the effects of the fiber orientations, cutting force along with the cutting conditions, the chip occurrence mechanisms, the debonding in the interface, and the sub-surface damage. The cutting force and thrust force were applied for various fiber orientations (15°, 30°, 45°, 60°, 75°, 90°), depth of cuts (0.1, 0.15, 0.2 mm) and rake angle (5°, 10°, 15°). They found out that the fiber orientation and depth of cut have

an effect on the increase of the cutting force, but the rake angle effects are less. Venu Gopala *et al.* [33] applied a 3-dimensional FEM model can predict cutting forces, occur surface defects and chip occurrence mechanisms when UD-CFRP was cut with different fiber orientation, depth of cut and tool rake angle.

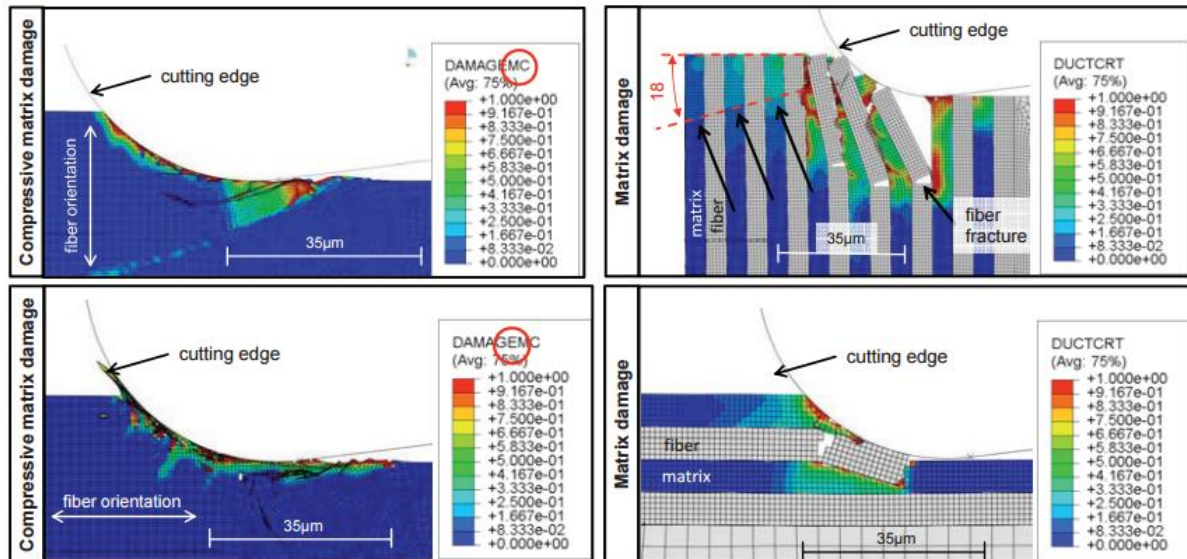


Fig. 2-9. Calculated matrix damage distributions in the macroscopic model (left) and the microscopic model (right): top row for a fiber orientation of  $90^\circ$  and bottom row for  $0^\circ$  fiber orientation [32].

A. Mkaddem and Mansori investigated the FEM model that applied adapting mesh technique and dynamic explicit, which were used to simulate the chip occurrence during the UD-GFRP orthogonal cutting [34]. The maximum sub-surface damage value was observed in  $90^\circ$  fiber orientation. A discrete element method was developed by Iliescu *et al.* [35]. They simulated the orthogonal cutting of UD-CFRP with  $0^\circ$ ,  $45^\circ$ ,  $90^\circ$  fiber orientations. To increase the simulation accuracy, they implemented the experimental cutting tests, reproducing experimental aspects about cutting forces and chip formation. They validated FEM model results by the high speed camera.

Calzada [20] worked comparison about the failure mechanisms when UD-CFRP was cut in the various fiber orientations ( $0^\circ$ ,  $45^\circ$ ,  $90^\circ$  and  $135^\circ$ ). The FEM model was developed with the ABAQUS based in the failure theories, and was able to explain the failure mechanisms that took place by the chip occurrence process for each fiber orientation. To validate chip formation, the experimental cutting process was worked, which was discovered representing the chip occurrence process. Sntiuste *et al.* [27] validated the FEM analysis by ABAQUS/Explicit. Inducing the surface damage was observed by the FEM model when the GFRP and CFRP was cut.

Rentsch *et al.* [36] created simulation model of CFRP materials. They used Hashin failure criteria in the FEM model that was used to predict at  $0^\circ$  and  $90^\circ$  fiber orientations. They observed surface damage



in the 90° fiber orientation and no cracks in the 0° fiber orientation after the cutting processes. They observed the predicted chip occurrence mechanisms with the experimental cutting, but the cutting forces were underestimated. While the compressive strength of the material become over value and the material become degradation, the elements are removed. The material of the yield state stayed between the tool and the workpiece, and could carry compressive load. Rentsch *et al.* [37] made CFRP FEM model to foresee the material removal mechanisms in accordance with orthogonal cutting conditions. The calculated results well matched experimental results based on the material removal mechanism partially. However, measured cutting forces were importantly measured lower than the experimental results, although those tendencies were calculated perfectly in case of the explicit fiber/matrix model. When CFRPs carried compressive loads in the FEM model, the elements were deleted completely.

### 2.2.1 Failure criteria

The chip is generated by the deformation process when the failure occurs with the failure criteria setted parameter. The simulation of the FRPs was various failure criteria such as Hashin, Maximum Stress, Tsai-Hill, Tsai-Wu, Punk, etc. [25, 38, 39, 40].

The structures of the composite materials are calculated by the stresses at individual integration point in their coordinate system. And then, those are calculated by the failure criteria. The FRPs properties at the point are reduced according to the failure mode when any failure occurs.

The failure criteria such as Maximum Stress and Hashin permit the model to apply the different stiffness degradation at fractured nodes and that can make a prediction of the cutting force [30].

- The maximum stress criteria

$$e_1^t = \frac{\sigma_{11}}{X_T} \text{ for } \sigma_{11} \geq 0 \quad (2-1)$$

$$e_1^c = \frac{|\sigma_{11}|}{X_C} \text{ for } \sigma_{11} \leq 0 \quad (2-2)$$

$$e_2^t = \frac{\sigma_{22}}{Y_T} \text{ for } \sigma_{22} \geq 0 \quad (2-3)$$

$$e_2^c = \frac{|\sigma_{22}|}{Y} \text{ for } \sigma_{22} \leq 0 \quad (2-4)$$

$$e_3^t = \frac{\sigma_{33}}{Z_T} \text{ for } \sigma_{33} \geq 0 \quad (2-5)$$



$$e_3^c = \frac{|\sigma_{33}|}{Z_c} \text{ for } \sigma_{33} \leq 0 \quad (2-6)$$

$$e_4 = \frac{|\sigma_{12}|}{S_{12}} \quad (2-7)$$

$$e_5 = \frac{|\sigma_{23}|}{S_{23}} \quad (2-8)$$

$$e_6 = \frac{|\sigma_{13}|}{S_{13}} \quad (2-9)$$

The failure is occurred and the material is declined when  $e_{t,c} > 1$ , and the failure mode make fail respectively with different level of load.

- Hashin criteria

1. Tensile fiber failure ( $\sigma_{11} \geq 0$ )

$$(e_1^t)^2 = \left( \frac{\sigma_{11}}{X_T} \right)^2 + \frac{\sigma_{12}^2 + \sigma_{13}^2}{S_{12}^2} \begin{cases} \geq 1 \text{ failure} \\ < 1 \text{ no failure} \end{cases} \quad (2-10)$$

2. Compressive fiber failure ( $\sigma_{11} < 0$ )

$$(e_1^c)^2 = \left( \frac{\sigma_{11}}{X_C} \right)^2 \begin{cases} \geq 1 \text{ failure} \\ < 1 \text{ no failure} \end{cases} \quad (2-11)$$

3. Tensile matrix failure ( $\sigma_{22} + \sigma_{33} > 0$ )

$$(e_2^t)^2 = \left( \frac{\sigma_{22} + \sigma_{33}}{Y_T} \right)^2 + \frac{\sigma_{23}^2 - \sigma_{22}\sigma_{33}}{S_{23}^2} + \frac{\sigma_{12}^2 + \sigma_{13}^2}{S_{12}^2} \begin{cases} \geq 1 \text{ failure} \\ < 1 \text{ no failure} \end{cases} \quad (2-12)$$

4. Compressive matrix failure ( $\sigma_{22} + \sigma_{33} < 0$ )

$$(e_2^c)^2 = \left[ \left( \frac{Y_C}{2S_{23}} \right)^2 - 1 \right] \left( \frac{\sigma_{22} + \sigma_{33}}{Y_C} \right)^2 + \frac{(\sigma_{22} + \sigma_{33})^2}{4S_{23}^2} + \frac{\sigma_{23}^2 - \sigma_{22}\sigma_{33}}{S_{23}^2} + \frac{\sigma_{12}^2 + \sigma_{13}^2}{S_{12}^2} \begin{cases} \geq 1 \text{ failure} \\ < 1 \text{ no failure} \end{cases} \quad (2-13)$$

5. Interlaminar tensile failure for  $\sigma_{33} > 0$

$$(e_3^t)^2 = \left( \frac{\sigma_{33}}{Z_T} \right)^2 \begin{cases} \geq 1 \text{ failure} \\ < 1 \text{ no failure} \end{cases} \quad (2-14)$$

6. Interlaminar compression failure for  $\sigma_{33} < 0$

$$\left(e_3^c\right)^2 = \left(\frac{\sigma_{33}}{Z_C}\right)^2 \begin{cases} \geq 1 & \text{failure} \\ < 1 & \text{no failure} \end{cases} \quad (2-15)$$

where  $\sigma_{ij}$  is the stress components, and T and C is defined the tensile and the compressive strengths for the lamina individually.  $X_T, Y_T$  and  $Z_T$  are the maximum tensile strengths and  $X_C, Y_C$  and  $Z_C$  are the maximum compressive strengths in the three directions of the material.  $S_{12}, S_{13}$  and  $S_{23}$  are shear strengths in the principal material directions respectively [41, 42]. Hashin criteria are similar to maximum stress criteria when the failures exceed 1, the failure take place at the nodes of the material points and reduced model is applied. Each failure mode make fail respectively at various load grade.

The simulations used the failure criteria, Maximum Stress and Hashin failure criteria, present the elastic properties by three components; FV1, FV2 and FV3, which components are the matrix failure, the fiber failure and the fiber-matrix interface failure.

The Hoffman criterion can't present the failure orientation. Therefore, the no various stiffness degradation must be applied. While the Hoffman criterion is an appropriateness, all stiffness are reduced

- Hoffman criterion

$$e_{Hoffman} = \frac{e_{11}^2}{X_t X_c} + \frac{\sigma_{11} \sigma_{22}}{X_t X_c} - \frac{\sigma_{22}^2}{Y_t Y_c} + \frac{X_t + X_c}{X_t X_c \sigma_{11}} + \frac{Y_t + Y_c}{Y_t Y_c \sigma_{22}} + \frac{\sigma_{12}^2}{S_c^2} \geq 1 \quad (2-16)$$

when the failure criterion exceeds 1, this value remains until the end of the cutting process, and the chip formation is completed. While the failure is occur along with the reduced model applied, the mechanical properties are changed.

### 2.2.2 Cohesive zone model

The mechanical model needs called the cohesive zone model (CZM) for the model development, which is the region such as chip formation area [43, 31, 32].

Calzada [20] studied the failure mechanisms in the micro-scale when CFRPs cutting of the various fiber orientations;  $0^\circ, 45^\circ, 90^\circ$ , and  $135^\circ$ , which the diameter of the fibers is  $5\sim 8 \mu\text{m}$  and the fiber volume fraction was 60%. The matrix was modelled with the isotropic material which the fibers consisted of an anisotropic elastic material. The simulation model of CFRPs was used by ABAQUS

that can simulate advanced damage model. The Calzada simulation showed the cutting force and fiber failure, and figure 2-10 shows the fiber failures.

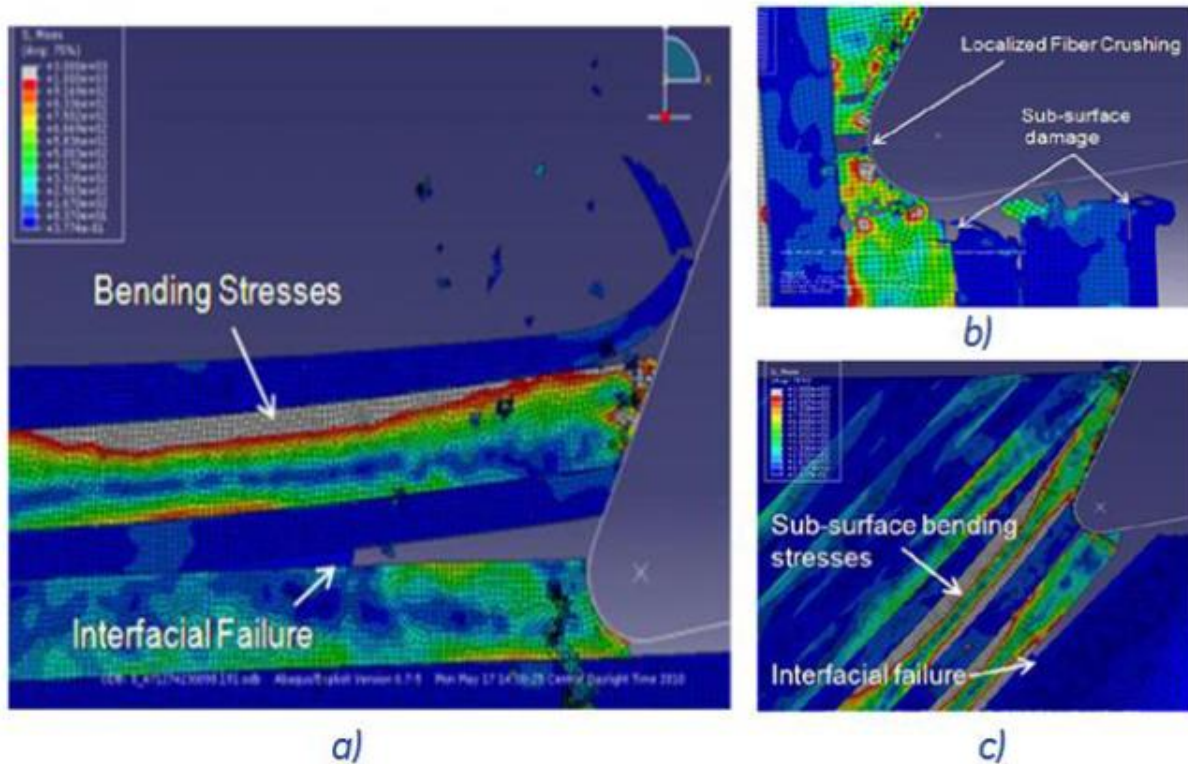


Fig. 2-10. Simulation results for different fiber angles workpiece (a) 0° (b) 90° (c) 135° [21]

The workpiece of the 0° fiber orientation showed the separation of the matrix-fiber because of the interface failure which generates chip formation as soon as the tool enters the workpiece. The bending occurs along with the cutting tool until the fiber failure in the vertical direction of the fiber direction. They are shown that the chip formation was occur come off the point of the contact to the tool when the 0° fiber was cut. While simulating the 45° and 90° fibers, the fibers smash as the tool contacts CFRPs, and which was shown in figure 2-10 (b). The bending stresses generate under the cutting surface, but the damage such as the delamination was occurs between fiber and the matrix. When the 135° fiber orientation was cut by the tool as shown figure 2-10 (c), the fibers were peeled in the tool front because of the failure the interface of the fiber and matrix under the cutting surface. After CFRPs were cut, the fiber peeling and fiber failure were generated by the bending stress on the cutting surface. The cutting forces graph had many variations, and which had a high variability in the simulation of the 90° and 135° fiber orientations. Therefore, accurate prediction of cutting force was difficult in this machining simulation.

### 2.2.3 Carbon Fiber Reinforced Plastic (CFRP) drilling modeling

Vaibhav A. Phadnis *et al.* [44] developed the 3-dimensional FEM model of CFRP drilling. The FEM model can predict the drilling thrust forces and torque properly when those compared with results of the experimental cutting. The material model of drilling FEM model used user-defined material model according to a stress-based damage criterion in the laminar. The element removal method based on the limit stress levels in CFRPs was worked in the material model properly in CFRP drilling. They consisted of drilling FEM model with the cohesive zone elements between the composite laminar as shown figure 2-11, and which can predict the delamination in the inter-laminar. Delamination in the drill entry was reasonable, while the delamination shape as well as the size were slightly over-measured at the drill exit. They found out the optimal drilling cutting conditions in CFRP drilling with the FEM model. They observed that the thrust force, torque and delamination damage increase according to the feed rate, while degraded continuously by increasing cutting speeds.

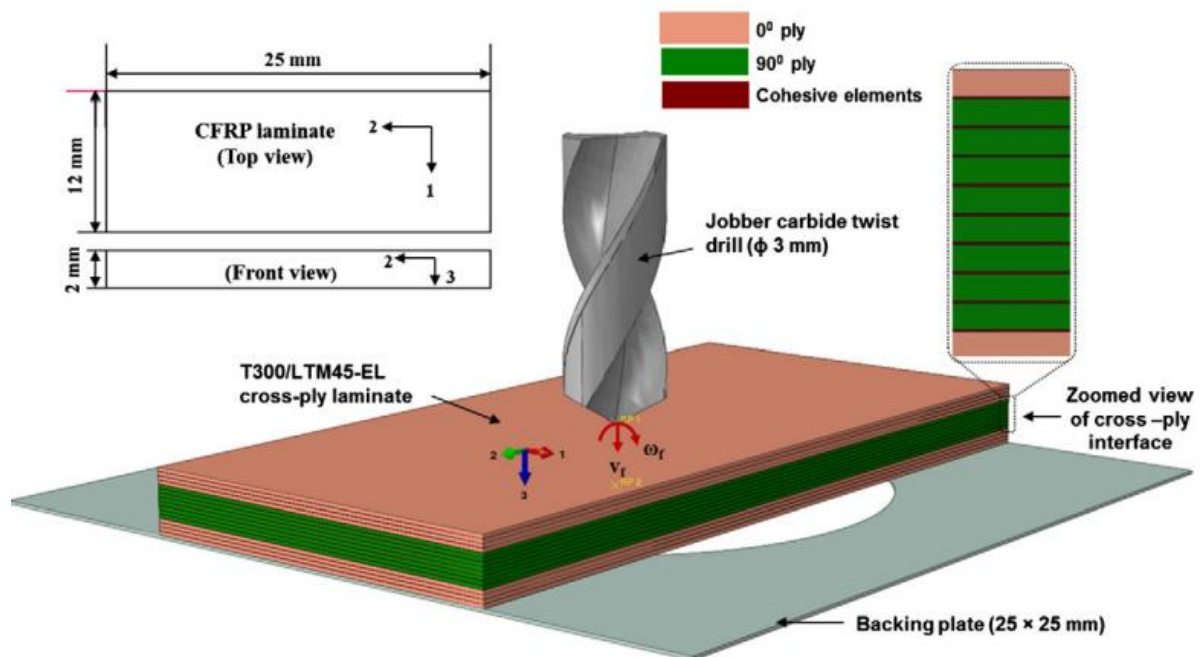


Fig. 2-11. Finite-element model of drilling T300/LTM-45EL CFRP laminate. (For interpretation of the references to color in this figure legend, the reader is referred to the web version of this article.) [44].

N. Feito *et al.* [45] developed the FEM model using two methods. Firstly, complete drilling model, including feed and rotation of the drilling was created. Secondly a simplified model, assuming that the drill acted such as a punch. These were compared about the delamination prediction. Developed model slightly overestimates the result of delamination factor. The simplified simulations present the results in several minutes, while completed model needs several days. They found out that the delamination

factor is increased when the thrust force is increased. The maximum delamination is same with the emerged by complete penetrating the workpiece with punch with similar drill geometry.

N. Feito *et al.* [46] were aimed to optimize drill geometry and process parameters to control machinability and investigate the drill wear after drilling process. They developed FE model using woven CFRP and the tool geometry of new and abrasion tools. They were able to estimate the thrust force and delamination in terms of abrasion and complex drills. Proposed model had presented estimate of damage and thrust force which were validated by using the experimental results.

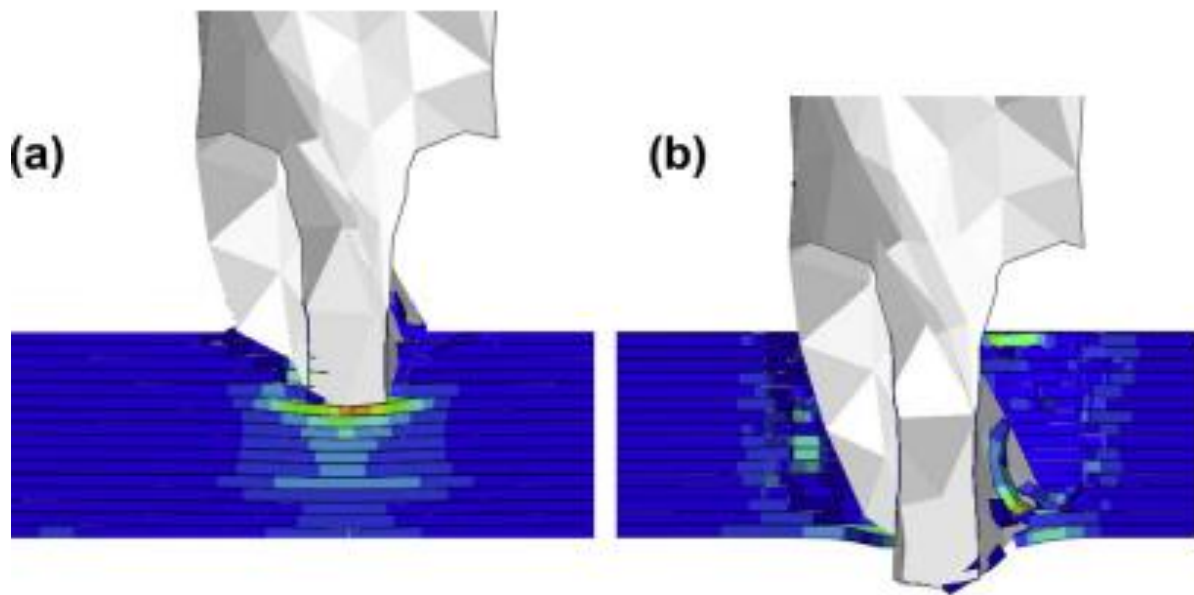


Fig. 2-12. Section of the hole during penetration of the drill simulated with complete model:  
 (a) entrance and (b) exit of the drill [45].

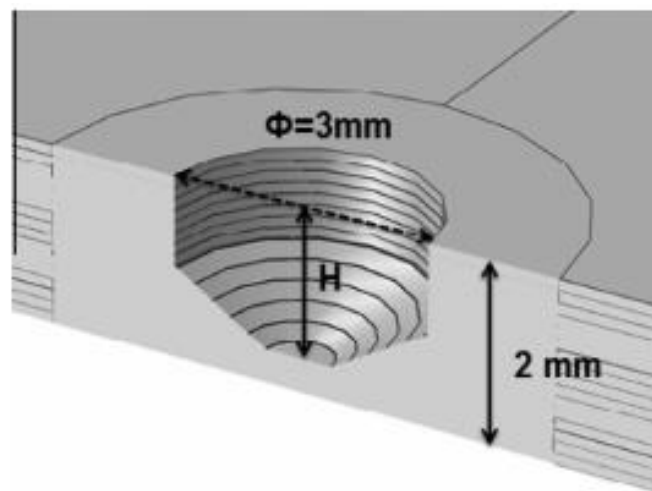


Fig. 2-13. Scheme of the pre-drilled hole in the simplified model [45].



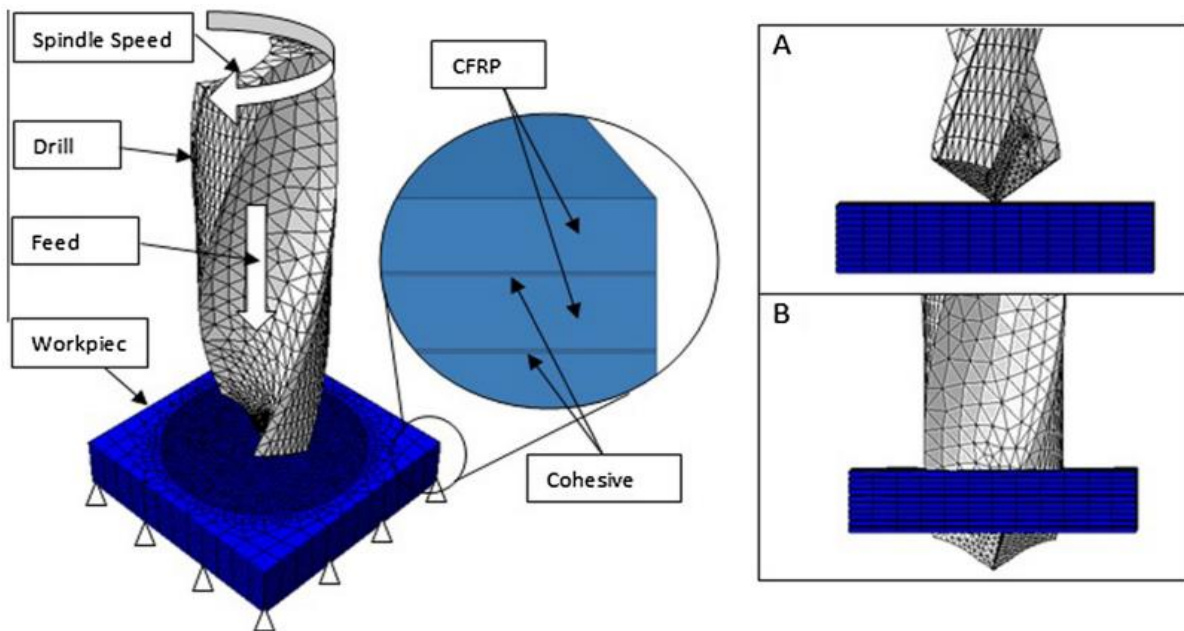


Fig. 2-14. Scheme of the complete model. Drill entrance simulation:  
 (a) initial and (b) final drill position [46].

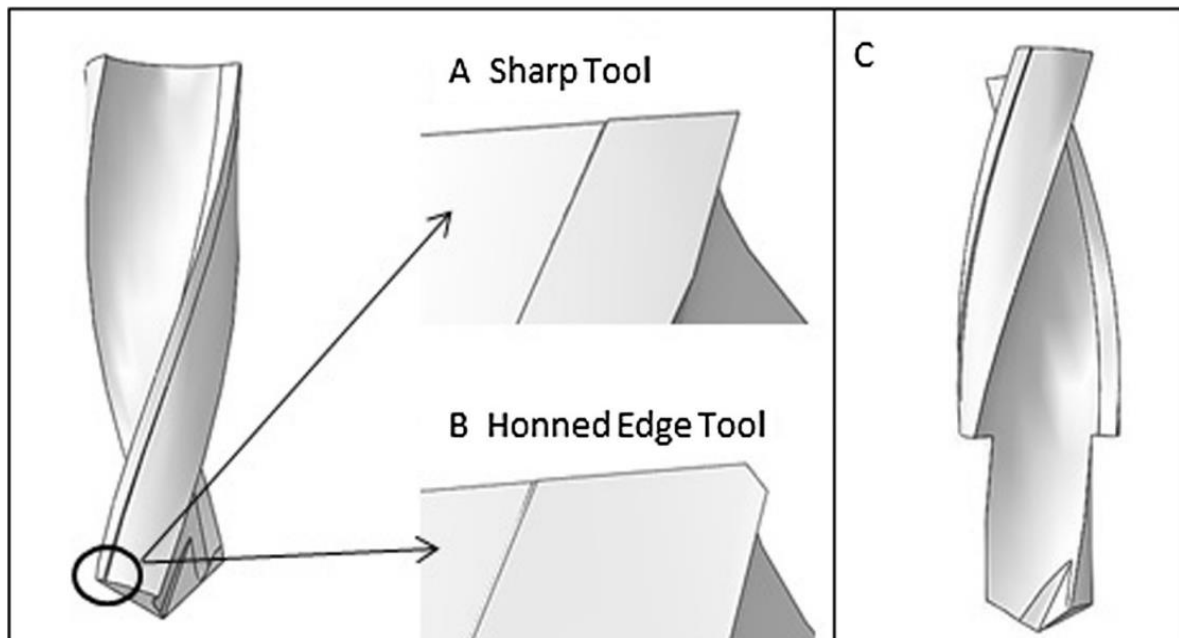


Fig. 2-15. Model of the geometries: (a) helical new (b) helical honed (c) and step [46].

### 2.3 Summary

In this chapter, we discussed existing researches dealing with CFRP cutting mechanisms and CFRP drilling simulations. CFRP cutting mechanism is different with that of metal cutting in that the chip morphologies are affected by fiber orientation: the chip morphology during CFRP cutting is dust type. During CFRP drilling, thrust force is defined as a key factor occurring delamination and fiber uncut. Therefore, the FE model has been commonly utilized in CFRP drilling modeling to find the thrust force. The FE model of CFRP drilling can find the chip morphology and defect such as delamination, fiber uncut, and so on.

### 3. CARBON FIBER REINFORCED PLASTIC DRILLING MODEL FOR PREDICTION OF DEFECTS

It is important to comprehend the influence of cutting conditions on CFRP to increase drilling process efficiency according to damage reduction. Many kind of the experimental researches were implemented in the past to optimize the cutting conditions so as to obtain better performance in CFRP drilling process. Some numerical models were also developed to define the critical thrust force in CFRP drilling process.

Finite element method (FEM) provides a system to develop an analytical model, which could reasonably show the CFRP drilling process and predict the corresponding levels of thrust force as well as delamination failure within a relatively reasonable computational time. When modeling and meshing the FE model, it is imperative to follow experimental conditions as closely as possible. In addition, it is essential to define some assumptions to simplify the model in order to speed up the analysis or even to make it executable for available computational resources in some cases. A proper balance between decreasing the computation time and increasing precision of results is able to be gained by an adaptive choice of factors like mesh size and shape. When verified, FE model is convenient and efficient to use for engineering works.

#### 3.1 FE model setup

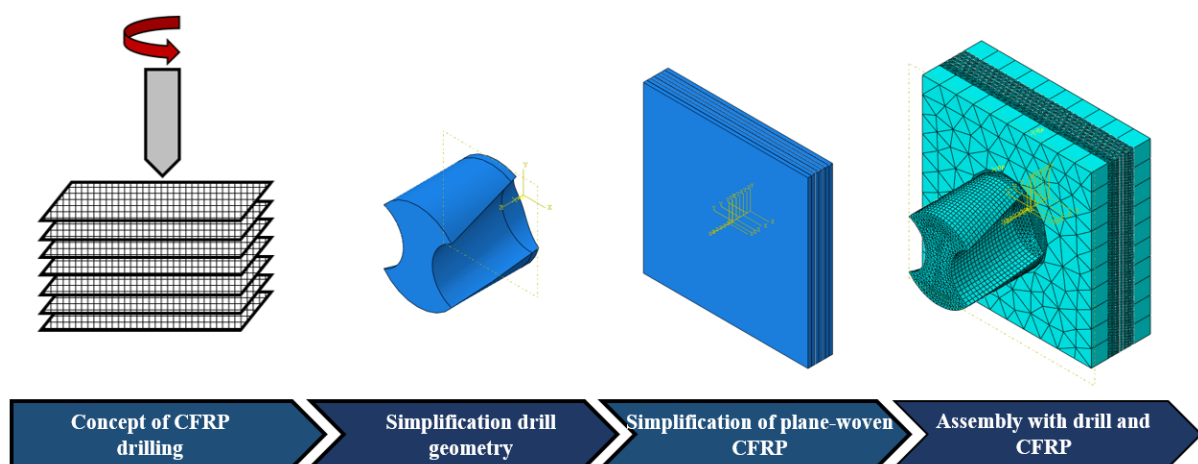


Fig. 3-1. Progress of Carbon Fiber Reinforced Plastic (CFRP) drilling simplification



A 3-dimensional FE model used commercial finite element software ABAQUS/Explicit. The simplification process of CFRP drilling for the 3D FEM modeling was shown in figure 3-1. This model aims to offer reasonable description of CFRP drilling process and to predict the corresponding levels of thrust force as well as delamination failure. This model aims to simulate the drilling of CFRP composites.

### 3.1.1 Geometry modeling

The drilling model consist of involve jigs as shown in figure 3-2. A specimen was used Plain-fabric CFRP, which consisted of the 14-plies in actual CFRP specimen. However, in FE model, whose thickness of ply is 0.429mm each ply has a dimension of 20 mm × 20 mm constitutes 7 plies with a stacking sequence of [0/90/0/90/0/90/0]. The reason of consisting the 7-ply is that we assumed the one ply in 2-plies. The coordination systems of each ply were defined to account for orientations of individual plies and to model the laminate and workpiece behavior precisely. The cohesive is used to surface based cohesive in the each CFRP ply interface, which cohesive thickness was defined 10 $\mu$ m.

The diameter of the drill used in experimental studies and FE model was 9 mm with 135° point angle and 30° helix angle. Used drill geometry in this simulation considered the reasonable element size, and defined as a rigid body that can decrease the general computational time in the high accuracy results. The used shape in drill bit point was plate to resolve the problem of overclosure that was shown in figure 3-4 (b). The drill had separation to two parts to reduce the calculation time as shown in figure 3-4 (b). The drill was fed into the workpiece in the axial direction using a velocity condition, which preforms the feed rate during experiments. An angular velocity about the drill axis equivalent to the spindle speeds of 5000rpm, 6000rpm and 7000rpm were imposed on all cases. Three sets of simulations were carried out with two different feed rates (0.04mm/rev, 0.06mm/rev) in each of three spindle speeds (5000rpm, 6000rpm, 7000rpm).]

The jig top and bottom to fix of fabric CFRP specimen were used in FE model. The dimension of each plate has 20 mm × 20 mm, and the thickness of each plate has 2mm. The jigs were defined to rigid body for reason like drill geometry type shown as figure 3-2. The top jig has  $\varnothing$  9.2mm hole, which are drill bush hole, and the bottom jig has  $\varnothing$  12mm hole to inspect such as defects of burr, uncut fiber and delamination after drilling.

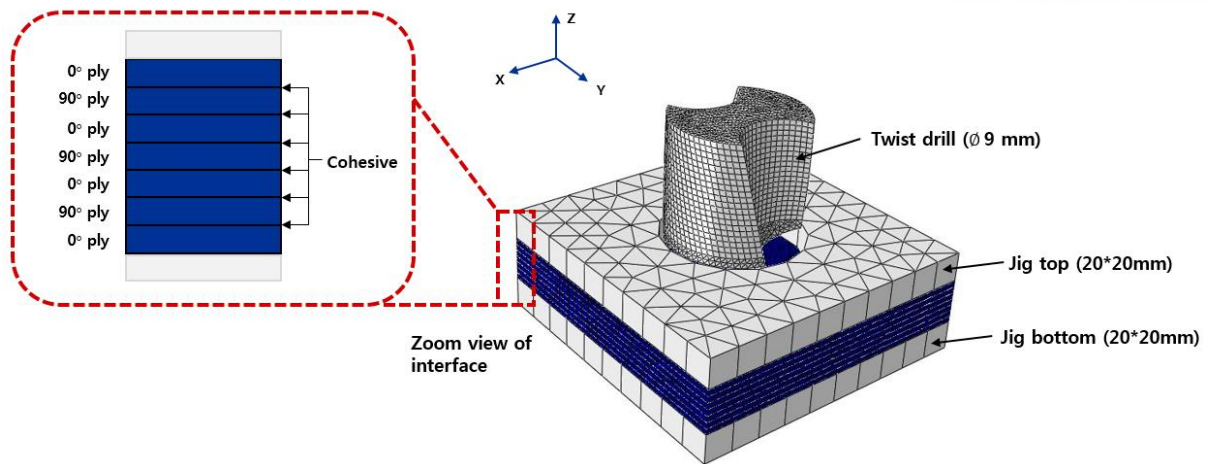


Fig. 3-2. Simplicity of FE model geometry

Table 3-1. Machining parameters in fabric CFRP.

Spindle speed (rpm)	5000		6000		7000	
Feed rate (mm/rev)	0.04	0.06	0.04	0.06	0.04	0.06

### 3.1.2 Boundary condition

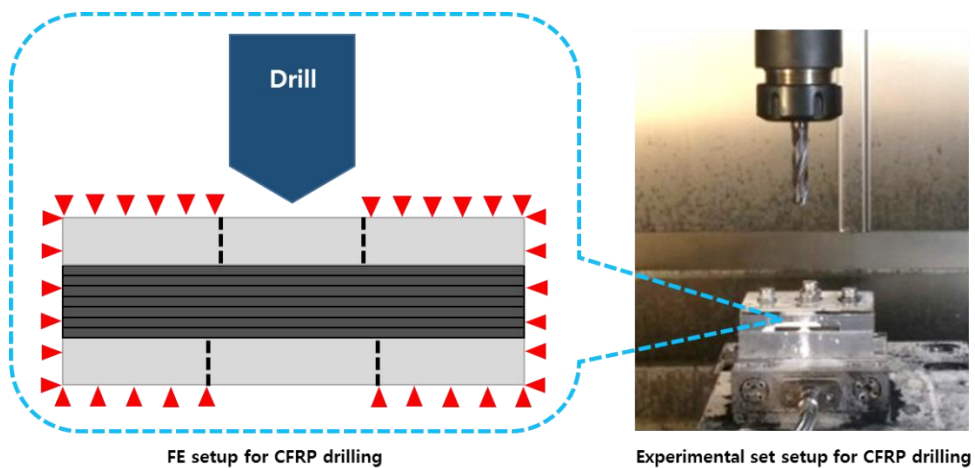


Fig. 3-3. Boundary condition of the FE model

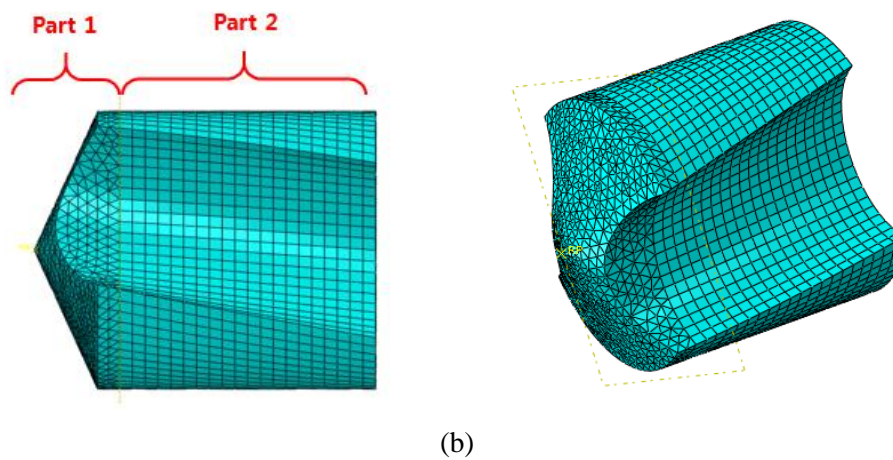
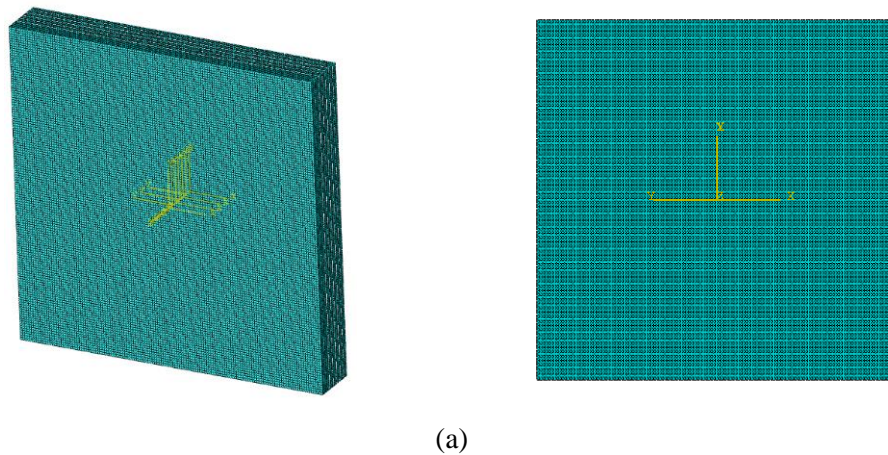
The boundary conditions in this FE model were described to the experimental setup as shown in figure 3-3. FE model used jig system, which fixed all face involving the jig and specimen. The jig was made to fix the CFRP specimen during CFRP drilling. The bottom side of the top jig was tied to the

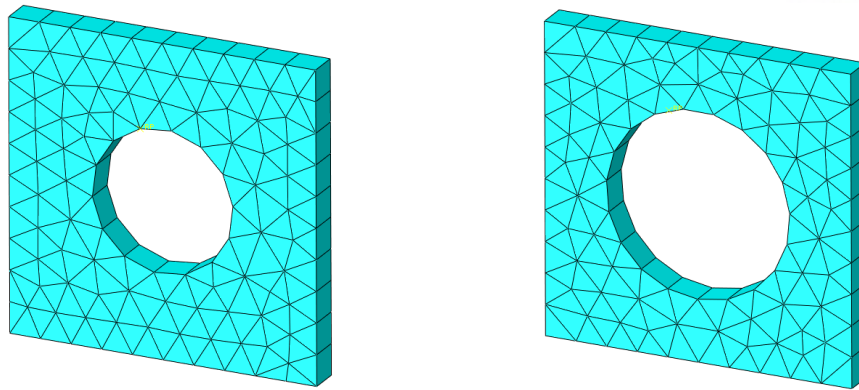
top side of the first CFRP ply, and the top side of the bottom jig was tied to the bottom side of the seventh CFRP ply applying for the tie constraint in order to describe the experimental boundary condition. All surfaces of jigs and CFRP specimen were fixed in boundary condition.

### 3.1.3 Element and mesh types

The elements and mesh size are critical in that computing time and analysis accuracy are closely related to them. The brick elements were used for fabric CFRP plate. The mesh type was C3D8R, an 8-node linear brick, and its global size was 0.15 in the fabric CFRP plates.

The mesh type of the drill was 3-node triangular shape and C3D6, which was a 6-node linear triangular, and it was refined with global size: 0.39 elements the part 1 of drill parts. The mesh type of the part 2 was rectangular shape: the swept type, which was defined with global size: 0.39 elements to reduce the computing time in part 2 as shown in figure 3-4 (b). Also, the jig mesh of top and bottom were swept type which consisted of global size: 2 elements as shown in figure 3-4 (c).





(c)

Fig. 3-4. Mesh of FE model (a) fabric CFRP (b) drill (c) jig top and bottom

### 3.2 Material property

The characteristic of the composite was anisotropic, which developed modeling applying for an elastic behavior to define failure. CFRP was typically modeled as a homogeneous material under the numerical cutting simulation. The Elastic properties of fabric composites were listed in Table 3-2 that involved that the values of fracture for inter laminar damage and included elastic stiffness, strength and fracture energy. Damage evolution was based on the Power law in mixed-mode. A user-define 3D of CFRP damage model (VUMAT) with solid elements was developed and implemented in ABAQUS/explicit [47] to predict the character and extent of damage through the laminate thickness. Interface Cohesive zones were inserted between the plies of the modelled laminate to simulate delamination. The general contact in ABAQUS/explicit was defined to simulate contact conditions between the drill and the carbon composite laminate, and between the layers by defining appropriate contact properties. An element deletion was used to the machining process based on damage initiation and damage evolution in the meshed CFRP elements. The cohesive was used as each ply interface model for delamination initiation and grew with the failure criterion in each ply interface. The detailed cohesive was explained in section 3.4.

Table 3-2. Properties of fabric CFRP.

$E_{11}=E_{22}$	$E_{33}$	$\nu_{12}$	$\nu_{23}=\nu_{13}$	$G_{12}$	$G_{23}=G_{13}$	$\rho$
61.5GPa	7.7GPa	0.05	0.3	3.7GPa	2.9GPa	1600kg/m <sup>3</sup>

### 3.3 Damage modeling

Damage modeling involves damage initiation as well as damage evolution (section 3.4), and which makes progressive damage and failure in cohesive layers that is defined.

FEM models are used to predict the failure as well as the damage. The method of laminate layup to the progressive failure in composite is layer-by-layer that has some advantages as followings:

- First, the three dimensional stress states can be considered.
- Second, the damage in the inter-ply can be found separately with the complex models visually.

Also, the damage initiation and propagation in composite material can be found by the element removal scheme in ABAQUS/explicit. An element was able to eliminate by the mesh when the stress levels are achieved until the limit levels.

The composite consists of some different physical components of the fiber and matrix. It has an heterogeneous property and brittle tendency. The cutting process of CFRP was confirmed in experimental studies (chapter 4). The brittle fracture mechanisms were dominated by fiber tensile failure, fiber compression failure, matrix tensile failure and matrix compression failure [48].

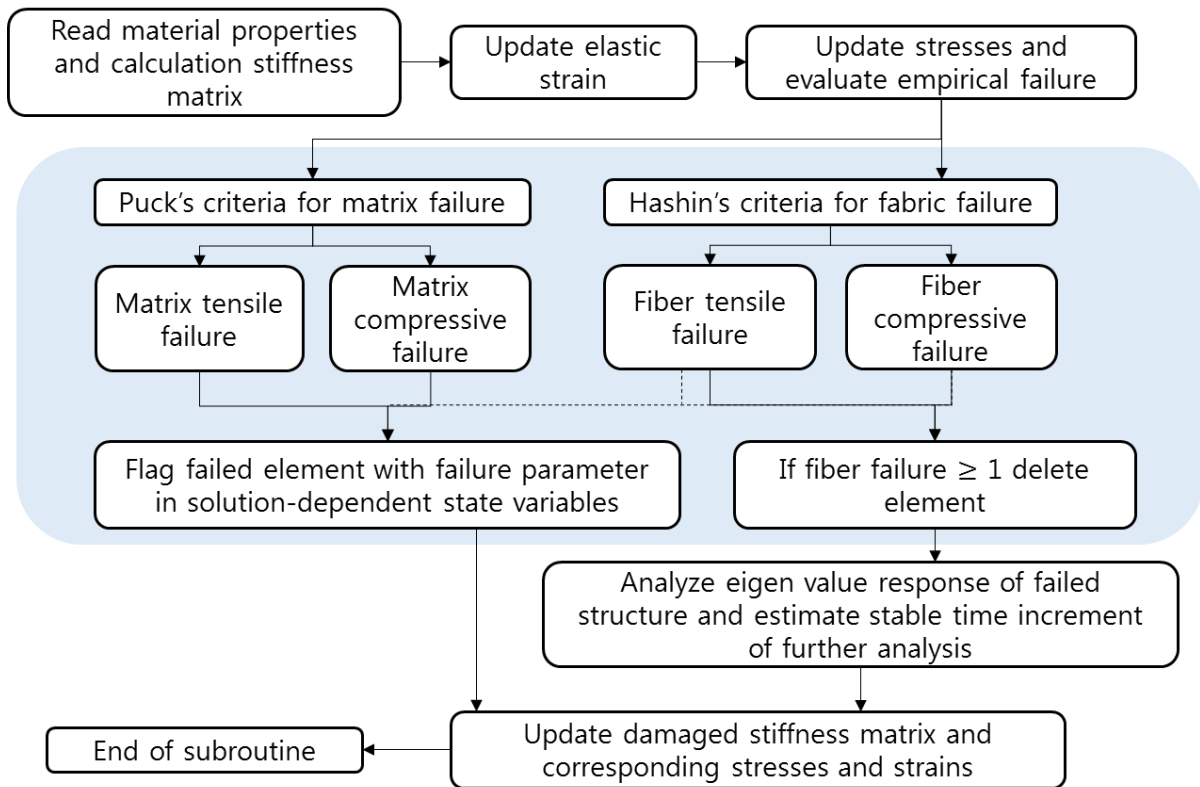


Fig. 3-5. Algorithm of VUMAT in ABAQUS/explicit [44]

Hashin damage model was used to the fiber reinforced composite materials to predict anisotropic damage. That related with different failure modes: both fiber damage in tension and compression and matrix tension and compressive failure. The damage model was used to the theory of Puck and Schurmann in this model that has shown the predictive capabilities for a number of failure criteria in composite laminates [49, 50]. In this study, the Hashin criteria were adopted to estimate in fiber damage, and the Puck failure criterion was utilized to the matrix failure model. The algorithm of VUMAT ABAQUS/explicit was presented in figure 3-5.

**Hashin criteria for failure in elastic fibers is defined with the following equation:**

[Fiber tensile failure ( $\sigma_{11} \geq 0$ )]

$$\left(\frac{\sigma_{11}}{S_{11}}\right)^2 + \left(\frac{\sigma_{11}}{S_{12}}\right)^2 + \left(\frac{\sigma_{11}}{S_{13}}\right)^2 = 1, \quad d_{ft} = 1 \quad (3-1)$$

[Fiber compressive failure ( $\sigma_{11} < 0$ )]

$$\left(\frac{\sigma_{11}}{X_{1c}}\right)^2 = 1, \quad d_{fc} = 1 \quad (3-2)$$

**Puck criteria for failure in brittle epoxy matrix are defined with the following equation:**

[Matrix failure]

$$\left[ \left( \frac{\sigma_{11}}{2X_{1t}} \right)^2 + \frac{\sigma_{22}^2}{|X_{2t}X_{2c}|} + \left( \frac{\sigma_{12}}{S_{12}} \right)^2 \right] + \sigma_{22} \left( \frac{1}{X_{2t}} + \frac{1}{X_{2c}} \right) = 1 \quad (3-3)$$

$$\sigma_{22} + \sigma_{33} > 0, \quad d_{mt} = 1$$

$$\sigma_{22} + \sigma_{33} < 0, \quad d_{mc} = 1$$



where  $\sigma_{11}$ ,  $\sigma_{22}$ ,  $\sigma_{33}$  and  $\sigma_{12}$  are defined with components of the stress tensors at an integration point of an element, and  $d_{ft}$ ,  $d_{fc}$ ,  $d_{mt}$  and  $d_{mc}$  are the damage variables related with failure modes in fiber tension and matrix compression.  $X_{1t}$  and  $X_{2t}$  are tensile failure stresses, and tensile failure stress in fiber direction and  $X_{2c}$  is compressive failure stress in direction 2, and  $S_{11}$ ,  $S_{12}$  and  $S_{13}$  are defined as shear failure stresses. The parameters for the strength of Fabric-CFRP used in this FEM model are listed in table 3-3.

In drilling FEM analysis, the element deletion was occurred by the mesh, and to remove the elements was used to the value of damage variables as calculated from the eq. (3-1) to the eq. (3-3), which was used to distinct damage modes in the modelled CFRP materials. The element was removed when the condition of the maximum damages was met at all the points of some integration point area of the element. The damage value,  $d$  ( $d \in \max\{d_{ft}, d_{fc}, d_{mt}, d_{mc}\}$ ), was defined when  $d=1$ , the element was deletion from the mesh and no more resistance to deformation [51].

Table 3-3. Strength properties of fabric CFRP.

$X_{1t}=X_{2t}$	$X_{3t}$	$X_{1c}=X_{2c}$	$X_{3c}$	$S_{12}$	$S_{13}=S_{23}$
840MPa	50MPa	570MPa	70MPa	72MPa	100MPa

### 3.4 Delamination modeling

In the FE model, the delamination modeling in drilling simulation was occurred by the damage initiation criteria and damage evolution in ABAQUS/explicit. The criteria based on normal and shear stresses when the delamination initiated is defined as the following equation [52, 53]:

$$\left[ \frac{t_n}{t_n^0} \right]^2 + \left[ \frac{t_s}{t_s^0} \right]^2 + \left[ \frac{t_t}{t_t^0} \right]^2 = 1 \quad (3-4)$$

Where  $t_n$ ,  $t_s$  and  $t_t$  are the components of the normal traction stress and the shear traction stresses in the cohesive interface respectively, and  $t_n^0$ ,  $t_s^0$  and  $t_t^0$  are defined with the maximum values of those when the deformation is begun [51, 54]. The quadratic nominal stress criterion given in eq. (3-4) was used in this FEM damage modeling.

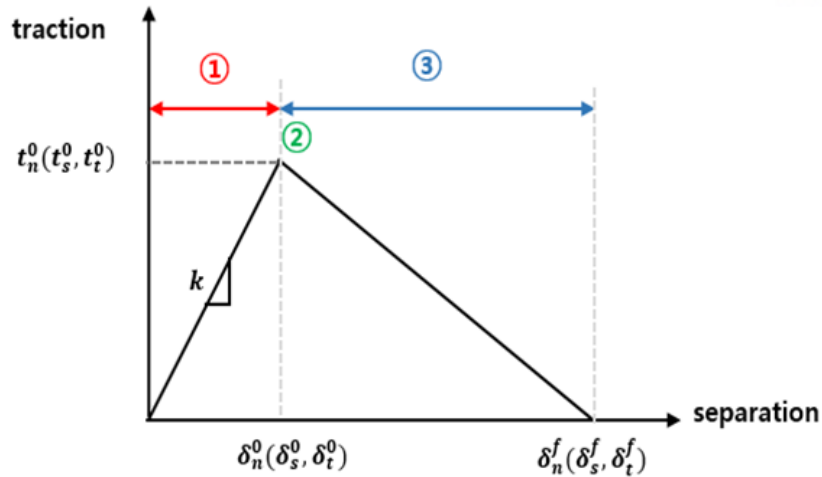


Fig. 3-6. Damage initiation, criterion and evolution in the interface cohesive.

The damage evolution with the potential, based on fracture energies which was based on mixed-mode, was used to a power law fracture criterion with the following equation:

$$\left[ \frac{G_n}{G_n^c} \right]^\beta + \left[ \frac{G_s}{G_s^c} \right]^\beta + \left[ \frac{G_t}{G_t^c} \right]^\beta = 1 \quad (3-5)$$

Where  $G_n$ ,  $G_s$  and  $G_t$  are the immediate fracture energies in normal and shear directions, and  $G_n^c$ ,  $G_s^c$  and  $G_t^c$  are the critical values of the fracture energies required to initiate failure in the normal, the first and the second shear directions, respectively. The interface cohesive was defined by a traction-separation law with mode- I failure as described in figure 3-5. The section ① described in figure 3-5 shows linear elastic behavior by the stiffness of the normal and the two shear directions ( $K_n$ ,  $K_s$  and  $K_t$ ), and it constantly increases till the peak value of the contact separation. At this section, damage does not occur. However, point ② of figure 3-5 describes damage initiation criterion, and its required traction stresses in the interface are nominated as  $t_n$ ,  $t_s$  and  $t_t$ . Section ③ in the figure 3-5 is the damage evolution by the critical fracture energy ( $G_n^c$ ,  $G_s^c$  and  $G_t^c$ ), and this section reveals stiffness degradation resulting from the damage evolution. The cohesive properties used in the interface were given in table 3-4.

Table 3-4. Material properties used in cohesive of the interface.

$K_n$	$K_s=K_t$	$G_n^c$	$G_s^c=G_t^c$	$t_n$	$t_s=t_t$	$\beta$
1GPa	1GPa	0.2N/mm	1N/mm	10MPa	20MPa	1



### 3.4.1 Contact conditions and friction coefficient

The contact condition and friction coefficient applied for FE model were determined by considering various experimental factors. They were cutting speed, feed rate, drill geometry and properties. The interaction between the drill and CFRP plies adopted general contact method which is available in ABAQUS/explicit which consisted on the basis of the penalty contact method. Therefore, friction test was performed by pin-on-disc test to find suitable the friction coefficient in drilling FE model without relation with the fiber orientation as shown figure 3-6. The equipment for friction test used UMT (Universal Mechanical & Tribology Tester), and tools used tungsten carbide tips (45°, 90°, 120°) for pin-on-disc test. All pin-on-disc tests were performed with friction test conditions presented in table 3-4. The results of the friction test are shown in figure 3-7 (b) and table 3-4. The friction coefficients of sharp tips like 45°, 90° initially tend to increase in the graph, since then friction coefficients are decreased and accepted by consistent value. In the comparison, the friction coefficient of the 120° tip slowly increased by 0.5. We assume that the sharp tips can rapidly penetrate to resin, that is why the coefficient of sharp tips are increased.

The drill geometry used in CFRP drilling are point angle 135°. Therefore, the friction coefficient between drill and CFRP laminates was set with constant coefficient of 0.5 to all FE simulations.

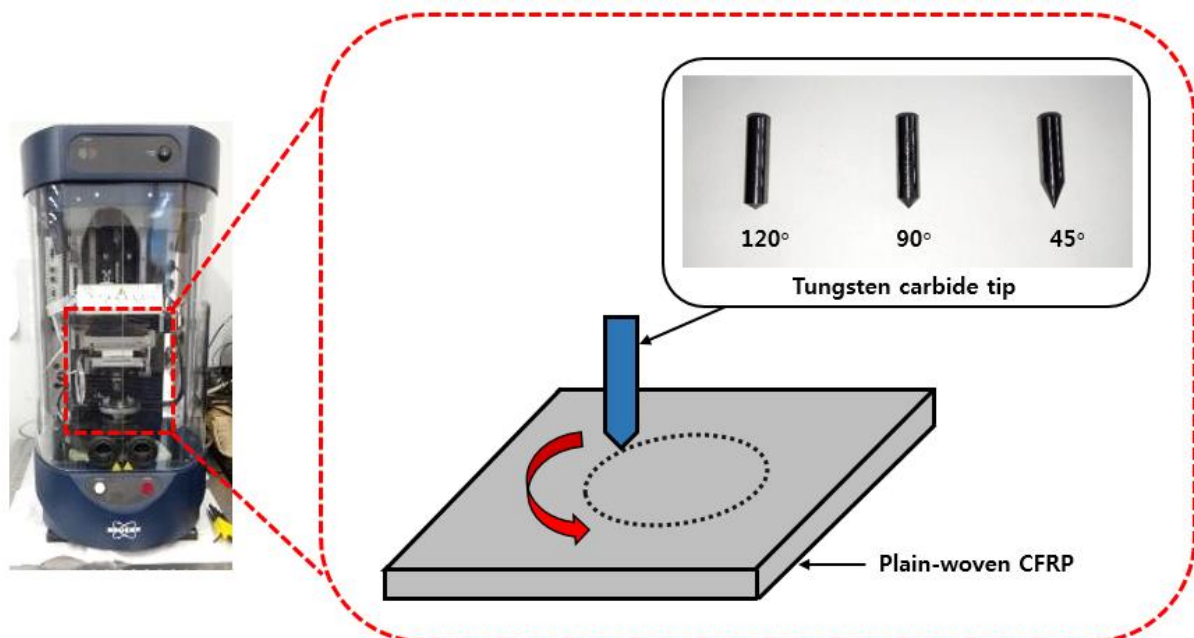
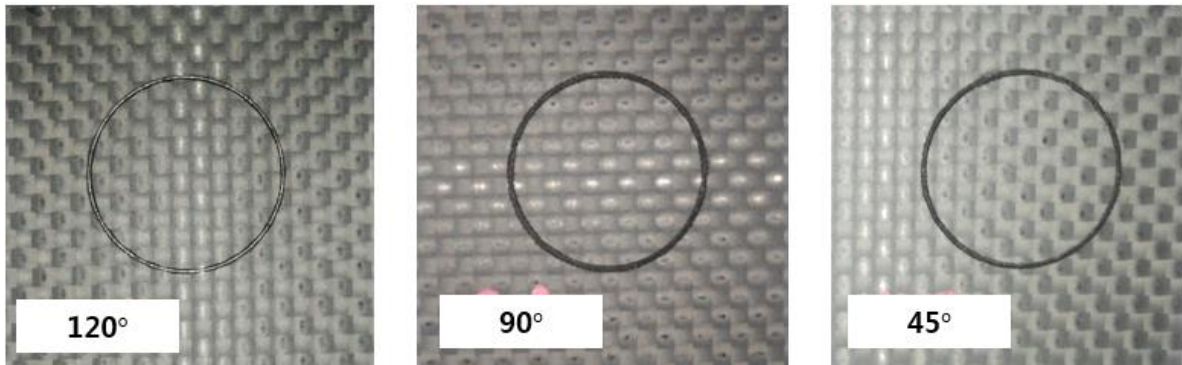
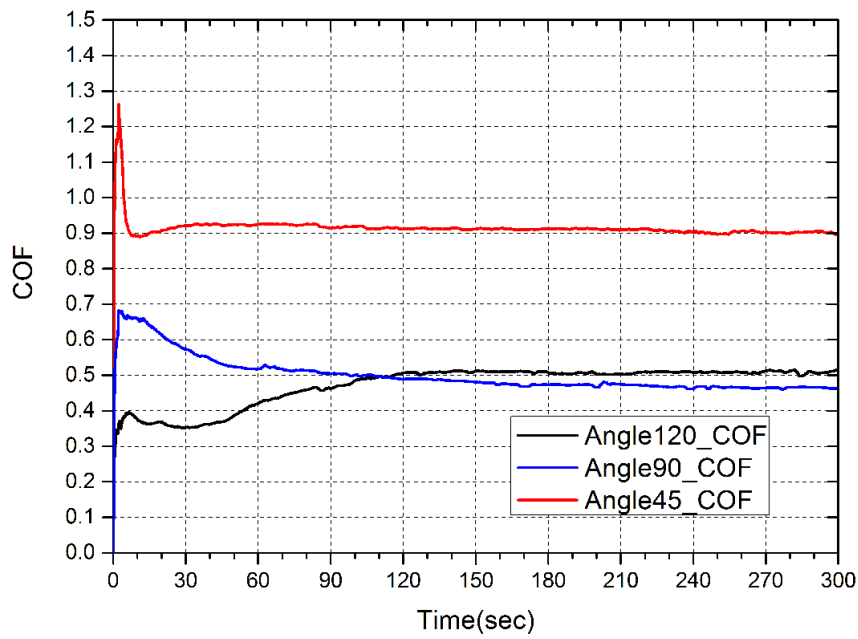


Fig. 3-7. Friction test (pin-on-disc test) setup



(a)



(b)

Fig. 3-8. Friction test (a) fabric CFRP specimens of friction test (b) friction coefficient result

Table 3-5. Pin-on-disc test conditions

Radius	Force	Time	Spindle speed
10 mm	10 N	5 min	100 rpm

### 3.5 Experiment setup

A machine setup for the experiments of CFRP drilling used the 5-axes CNC machine. The data of thrust force was obtained from a data acquisition system (KISLER, USA), and the dynamometer was 9257B type. The spindle speeds were 5000rpm, 6000rpm and 7000rpm with three different feed rates, presented in table 3-1. Thrust forces for the different machining conditions were obtained from the setting of figure 3-8.

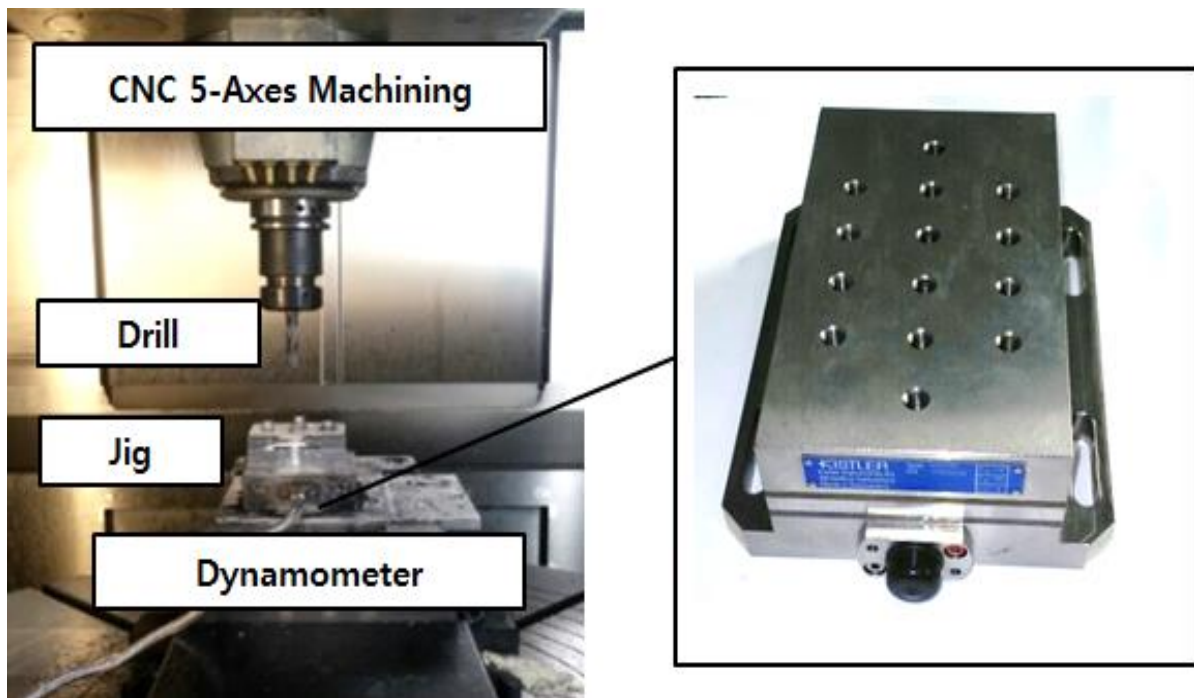


Fig. 3-9 Experimental setup for CFRP drilling

The tool as shown figure 3-9 (a) was B221 type (Kennametal) whose diameter is 9mm, and its helix angle is 30°. CFRP specimens whose thickness were ~3mm consist of T300-3k-plain-fabric carbon fiber that consisted of 14-ply and epoxy (SK chemical co.) as represented in figure 3-9 (b). Its size is 20\*20mm and its material properties were listed in table 3-2.

The fixture system used the customized jig systems to fix the CFRP specimen on the dynamometer as represented in figure 3-10. The fixture system consisted drill bush which helps guide, locate, and support the cutting tool. If this system use the drilling process, a hole accuracy can be increased.

ABAQUS/explicit is selected for simulation tool to predict the delamination of CFRP during the drilling to fulfill the aim of this study.

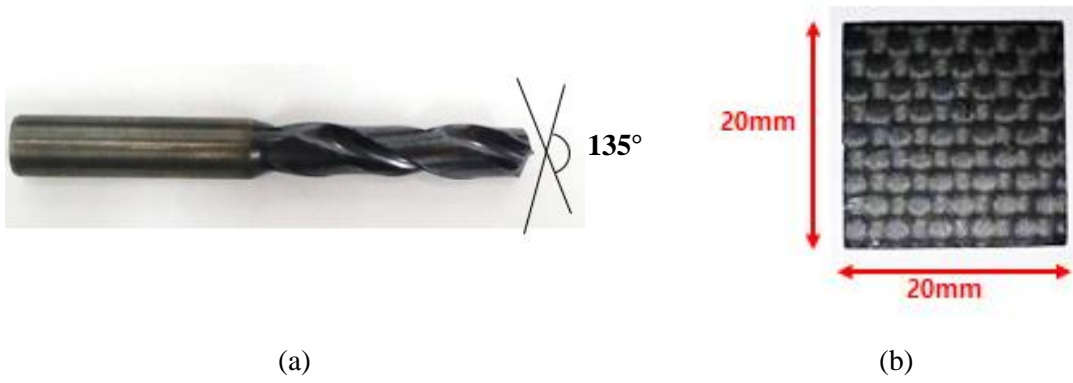


Fig. 3-10 (a) drill bit (b) fabric CFRP specimen for CFRP drilling

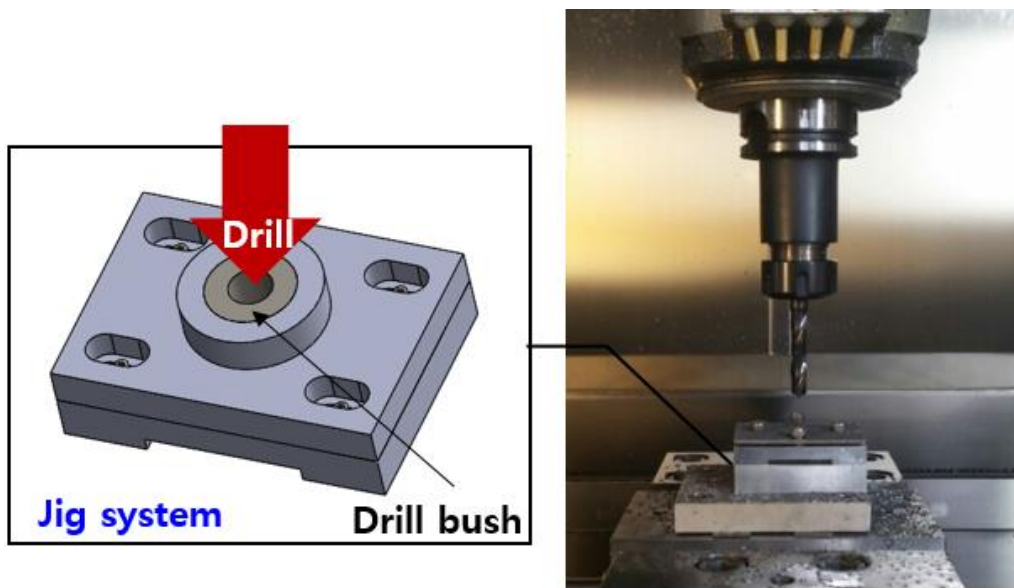
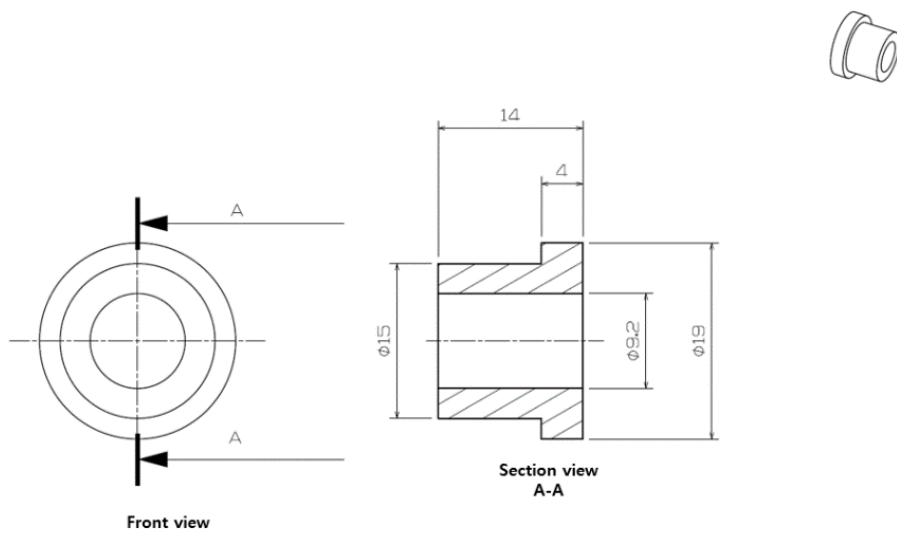
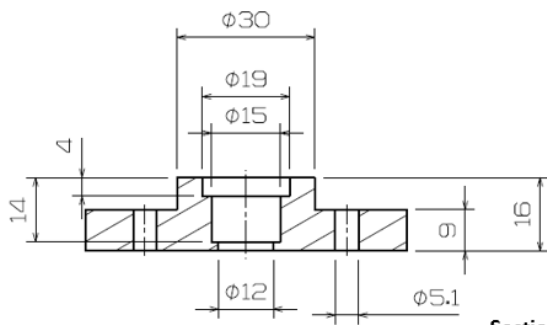
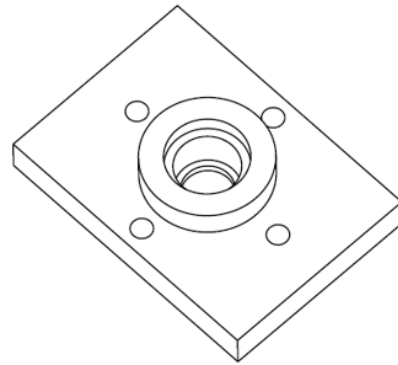
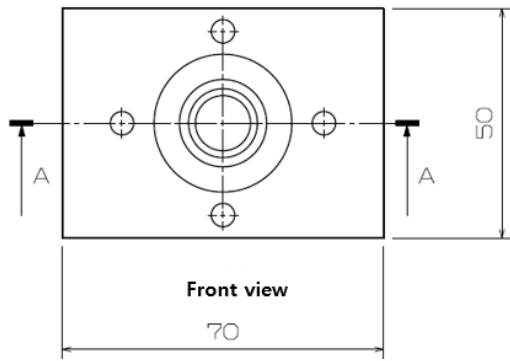


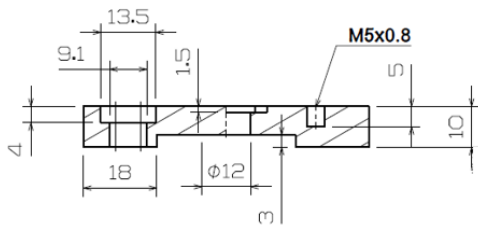
Fig. 3-11 CFRP drilling experimental setup



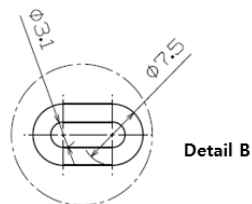
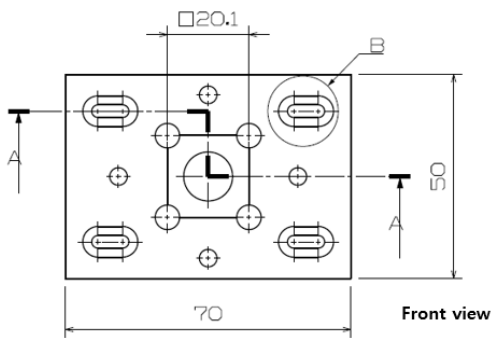
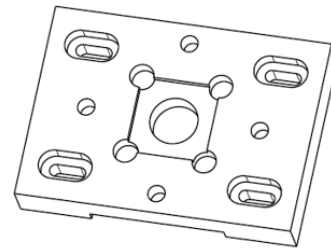


Section view  
A-A

(b)



Section view  
A-A



(c)

Fig.3-12 Design drawing of fixture systems (a) drill bush (b) jig top (c) jig bottom

### 3.6 Summary

In this chapter, the FE model for CFRP drilling was established. The authors composed the aforementioned setup in the FEM modeling, and simplified the drill geometry. The boundary conditions were set in CFRP plates, and the calculation time was considered in designating the elements and meshes. VUMAT in the 3D CFRP modeling was used for the material properties, which has the characteristics of an anisotropic composite. The damage modeling adopted a user-define 3D of CFRP damage model (VUMAT) defined as the Hashin criteria in the fiber and the Puck criteria in the matrix. The contact algorithm applied for the ABAQUS/explicit to describe delamination modeling in the interface cohesive. The contact friction between the drill and CFRP laminates were used as constant coefficients in the FE model. The experiment of CFRP drilling was carried on to verify the FE modeling with the results of the experiment.

## 4. VERIFICATION FINITE ELEMENT MODEL AND EXPERIMENTAL RESULTS

This chapter describes the verification of FE model developed which was compared with experimental results. The FE model was utilized to predict thrust force and defects, and the process is illustrated in figure 4-1. The experimental thrust force was measured by dynamometer and the defects such as the uncut fiber and hole quality of machined workpiece were investigated by SEM image or the naked eye. Also, FE model was used for understanding of thrust force. Those data were used when the verification of drilling simulation accuracy was done with the comparison of the results in drilling experiment.

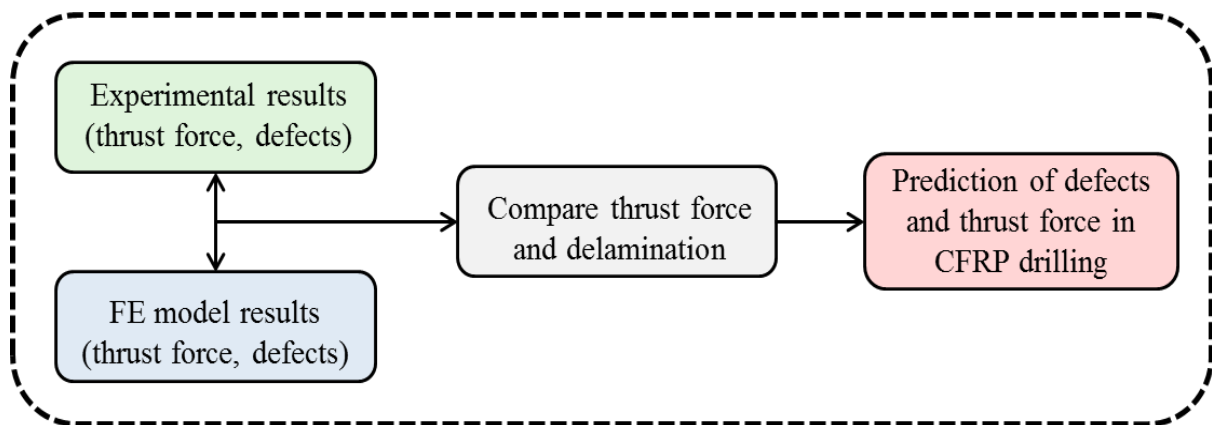


Fig. 4-1. Process to verify the FE model

### 4.1 FE model results of Carbon Fiber Reinforced Plastic (CFRP) drilling

FE model can understand drilling process and predict various factors such as defects and machining characteristics during drilling process. Furthermore, it can predict thrust force, delamination using stress contour, and hole machinability during drilling process. Developed FE model was verified from comparison of experimental results; thrust force graph, chip morphology, and machinability.



#### 4.1.1 Thrust force of FE model

Machining time of the drilling process is very short when making a hole. Therefore, we can't predict drill bit position during drilling process. However, FE model could show the drill position during the machining. Thrust force of FE model under CFRP drilling fluctuated up and down as shown in figure 4-2. Cutting condition was 5000rpm and feed rate was 0.06mm/rev. In this graph, thrust force increased when drill bit contacted CFRP specimen at first. Afterward, thrust force gradually increased at first to the maximum value. Then, thrust force gradually decreased by zero force.

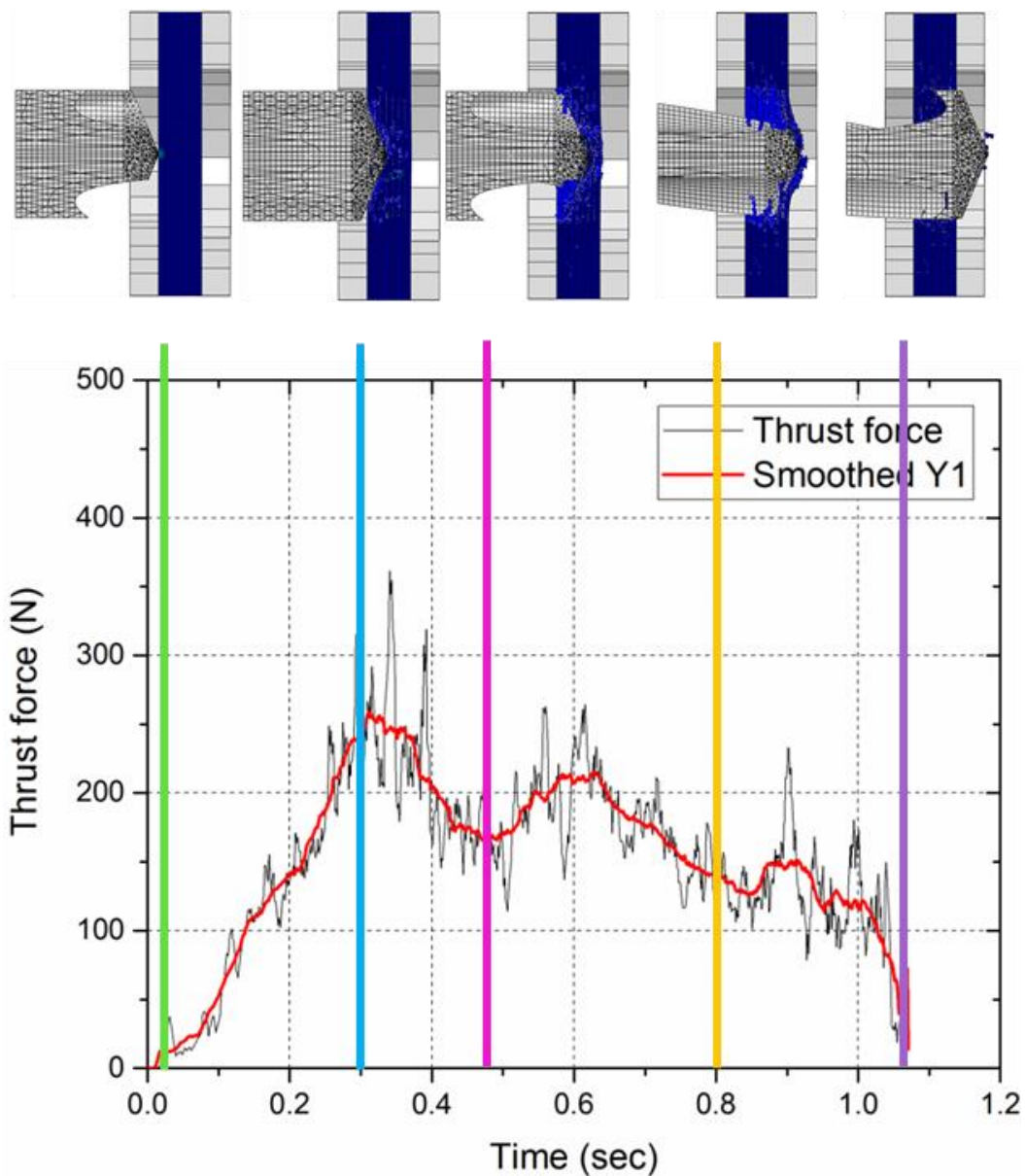


Fig. 4-2. Position of a drill bit under the drilling process



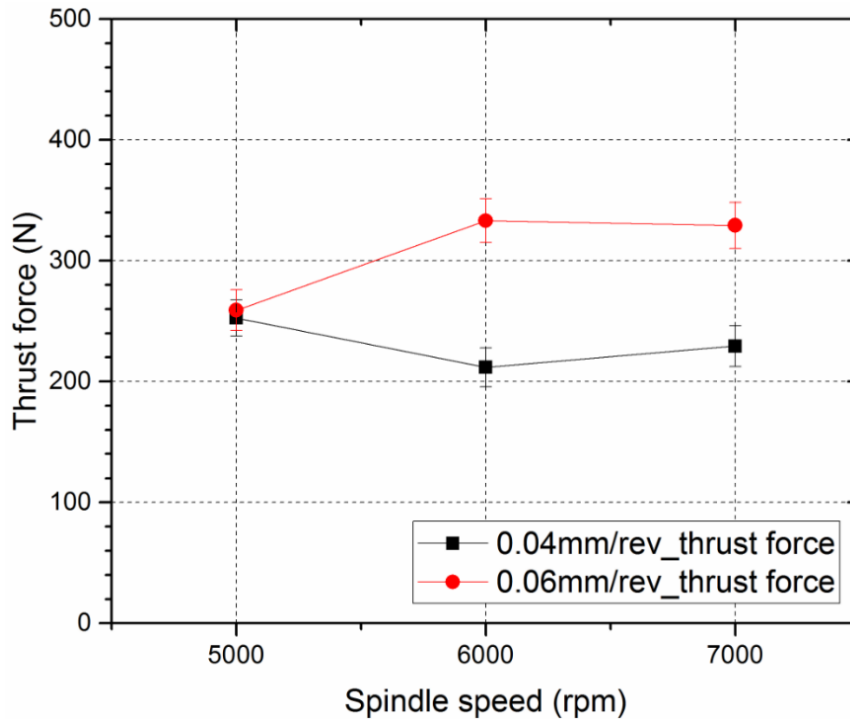


Fig. 4-3. Thrust force of CFRP drilling simulation

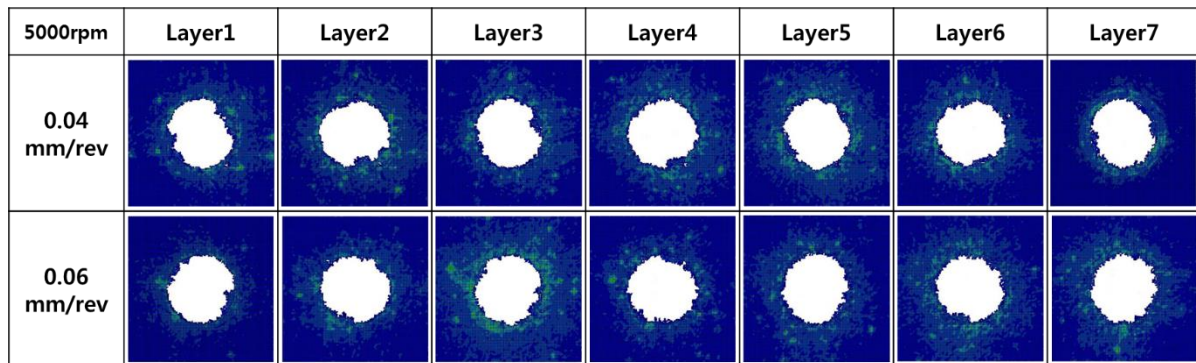
As a result of drill machining analysis using the developed FE model, the thrust force was obtained as shown in figure 4-3, and the numerical values in this graph are re-written in table 4-1. Cutting conditions of drilling process are presented in table 3-1. In this graph, the thrust force is almost similar to 0.04mm/rev and 0.05mm/rev of the feed rate in the cutting condition of 5000rpm spindle speed. However, there are difference thrust force of the spindle speeds of 6000rpm and 7000rpm. In those cutting conditions, thrust force with a feed rate of 0.06mm/rev was higher than low. Also, thrust force of spindle speed was higher than lower speed. Therefore, the thrust force tends to be influenced by the cutting condition.

Table 4-1. Thrust force in FE model of CFRP drilling

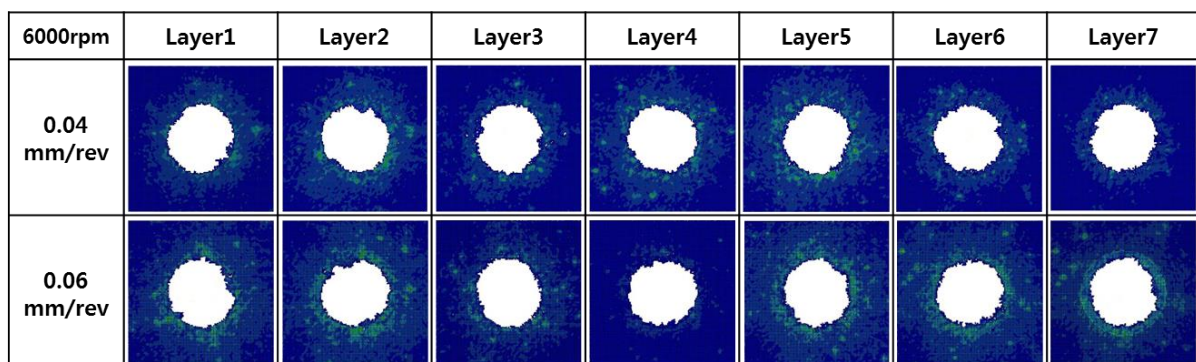
Spindle speed [rpm]	5000		6000		7000	
Feed rate [mm/rev]	0.04	0.06	0.04	0.06	0.04	0.06
FE model thrust force [N]	252.5	259.1	211.88	333.2	229.3	329.2

### 4.1.2 Stress contour of FE model

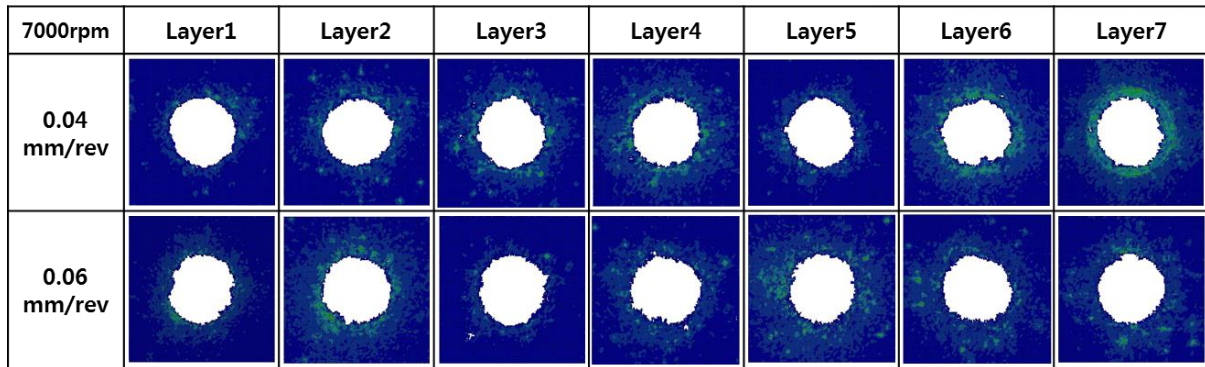
Delamination, inter-laminar debonding was observed in drilled CFRP specimen. It is difficult to detect delamination at inter-laminar region with naked eyes. However, FE model can predict and analyze the delamination which occurs between adjacent layers. Delamination in each layer could be identified by FE model as shown in figure 4-4. In this figure, stress contour was shown in the CFRP specimens and it represents delamination at inter-laminar regions. Besides, it is possible to identify hole machinability by using these pictures. In addition, it was proved that the best cutting conditions of hole machinability are as follows: cutting condition 7000rpm and feed rate 0.04 mm/rev which was used in these figures. Therefore, those stress contours proved that the hold quality becomes better when the cutting speed is higher and the feed rate is less.



(a)



(b)



(c)

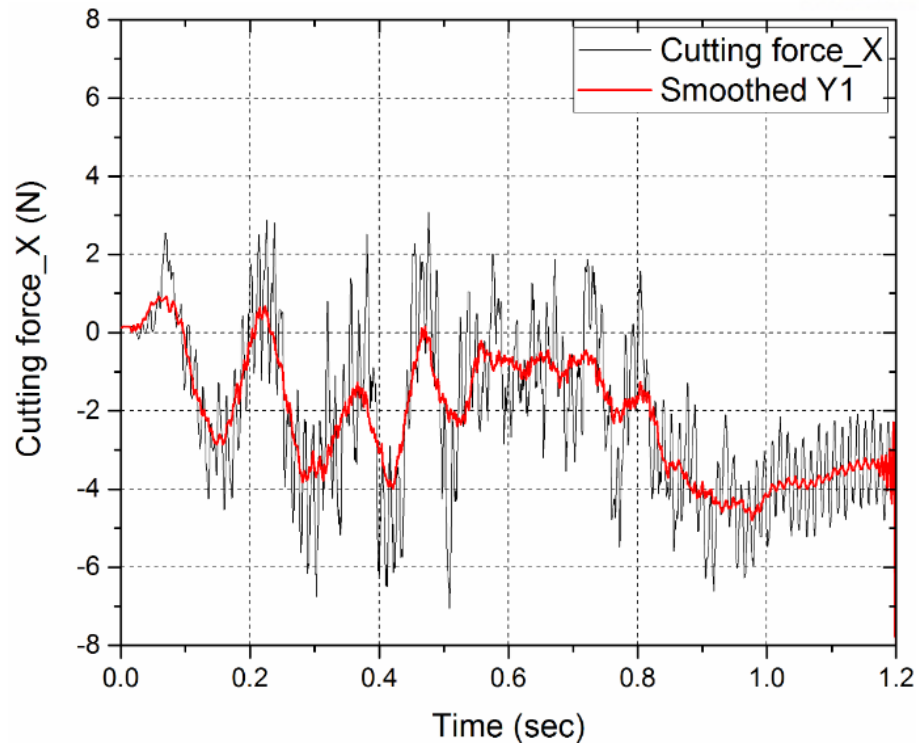
Fig. 4-4. Stress contour in CFRP drilling simulation (a) 5000rpm (b) 6000rpm (c) 7000rpm

## 4.2 Comparison FE model and experimental results

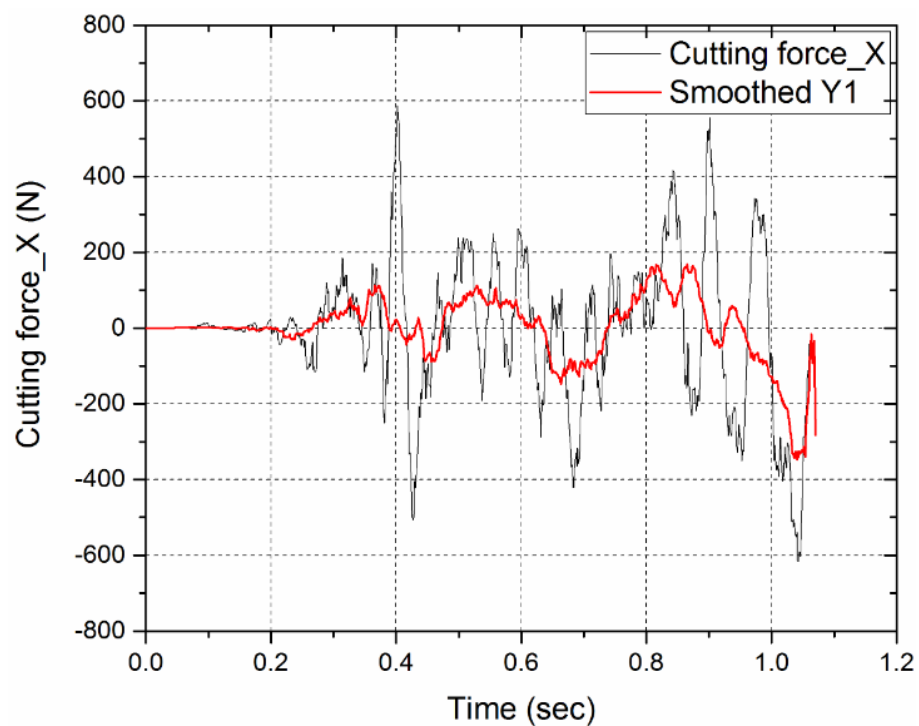
### 4.2.1 Thrust force

Forces of FE model and of experiment in CFRP drilling fluctuated up and down as shown figure 4-5 and 4-6. Cutting condition was 5000 rpm and feed rate was 0.06 mm/rev in these graphs, which looks similar to each other. Cutting force graphs of X and Y direction in the experimental results present sine curve in the figure 4-5 and 4-6. In addition, it was confirmed that the simulation results also show the same sine curve.

Thrust force graph also presents that the experimental result and the simulation result show similar graph as shown in figure 4-7. Thrust force gradually increased at first to the maximum thrust force value, and then gradually decreased, and finally it converged zero although a drill bit was machining the CFRP specimen as shown in figure 4-2. Thrust force is important factor related with the delamination in CFRP drilling process. Since the higher the speed in the feed direction, the higher the thrust force, which leads to delamination.

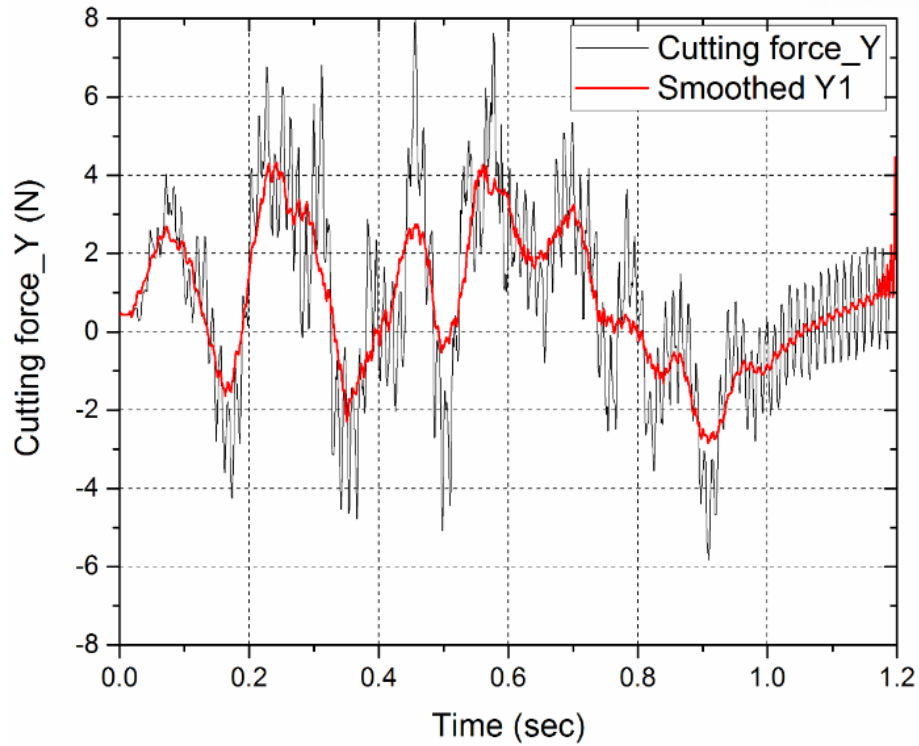


(a)

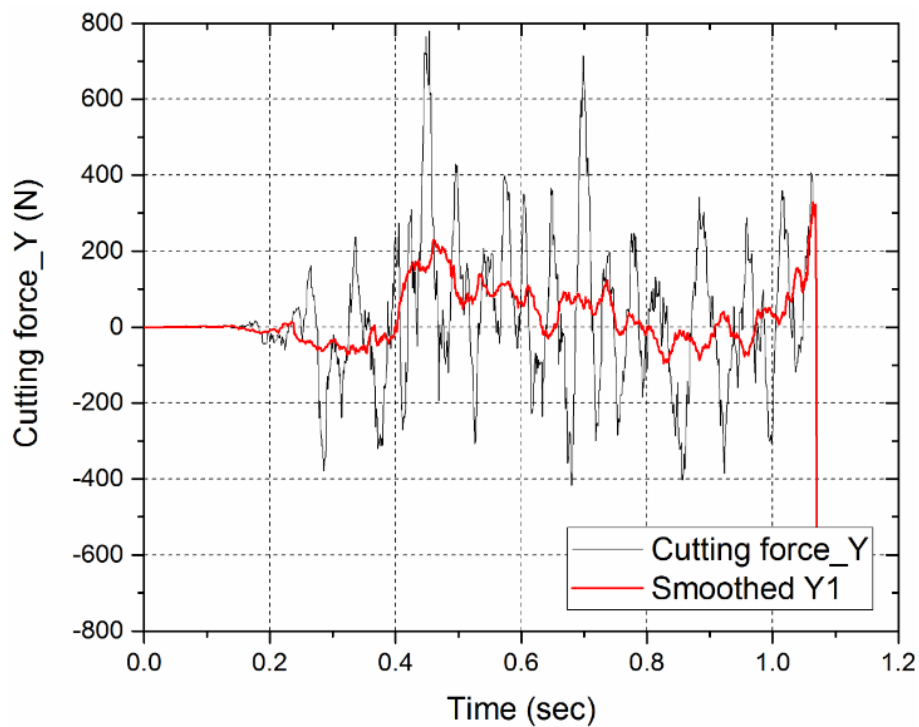


(b)

Fig. 4-5. Cutting force of X-direction (5000rpm, 0.06mm/rev) (a) experimental result (b) simulation result

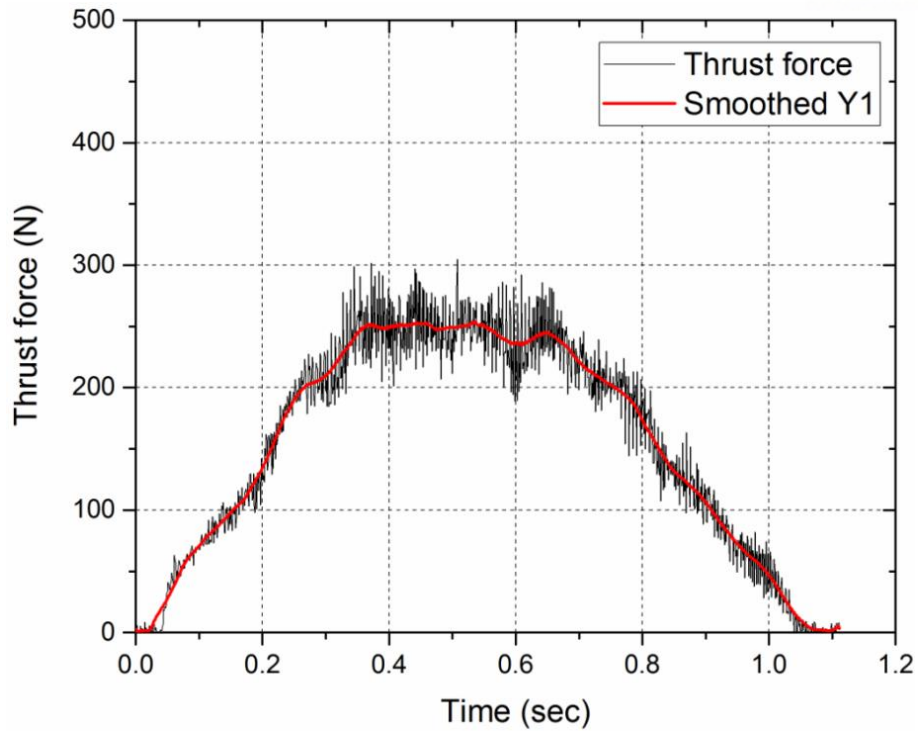


(a)

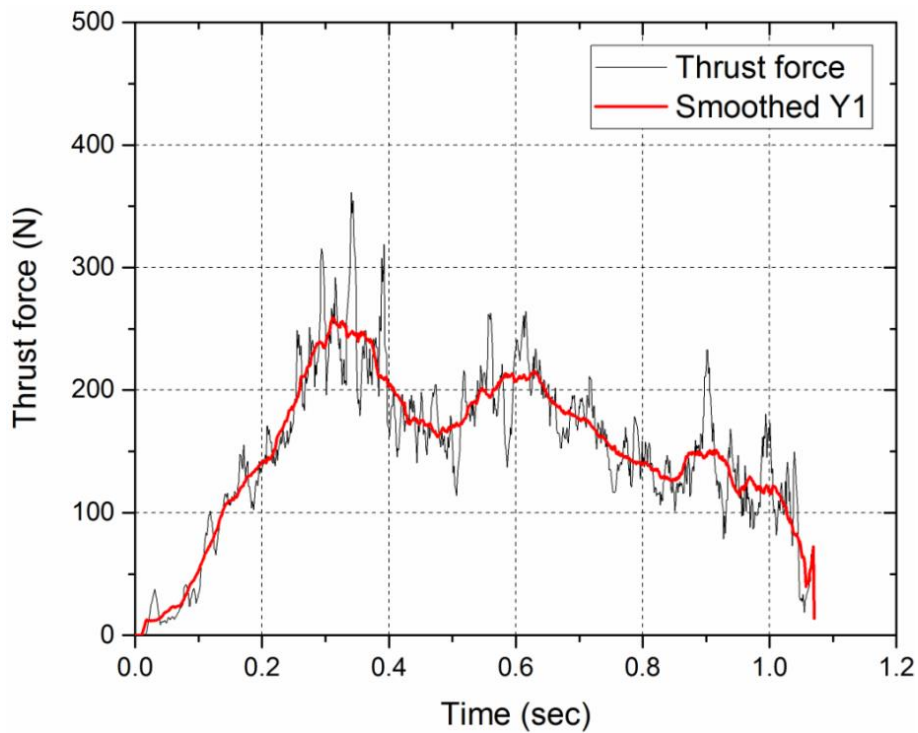


(b)

Fig. 4-6. Cutting force of Y-direction (5000rpm, 0.06mm/rev) (a) experimental result (b) simulation result



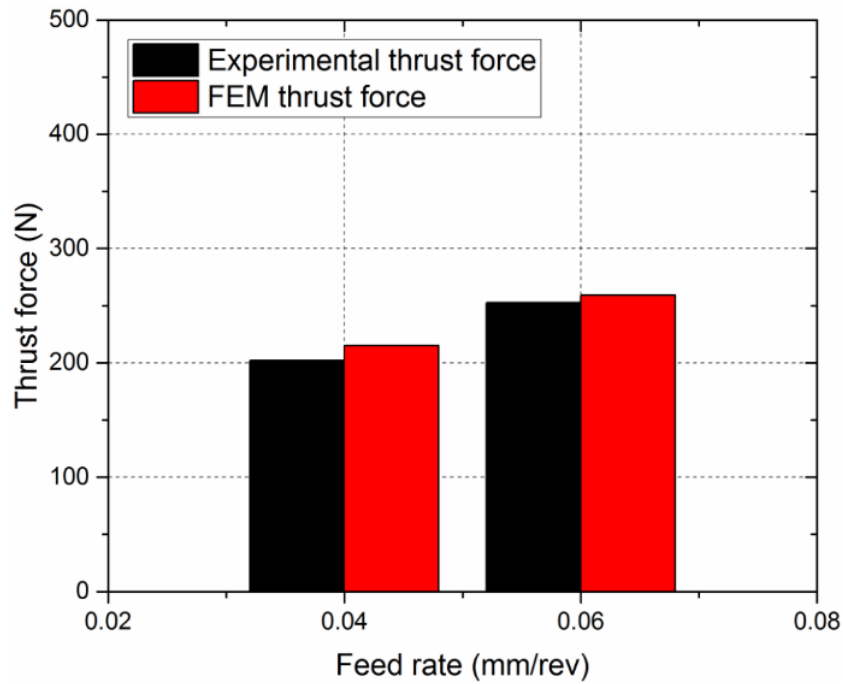
(a)



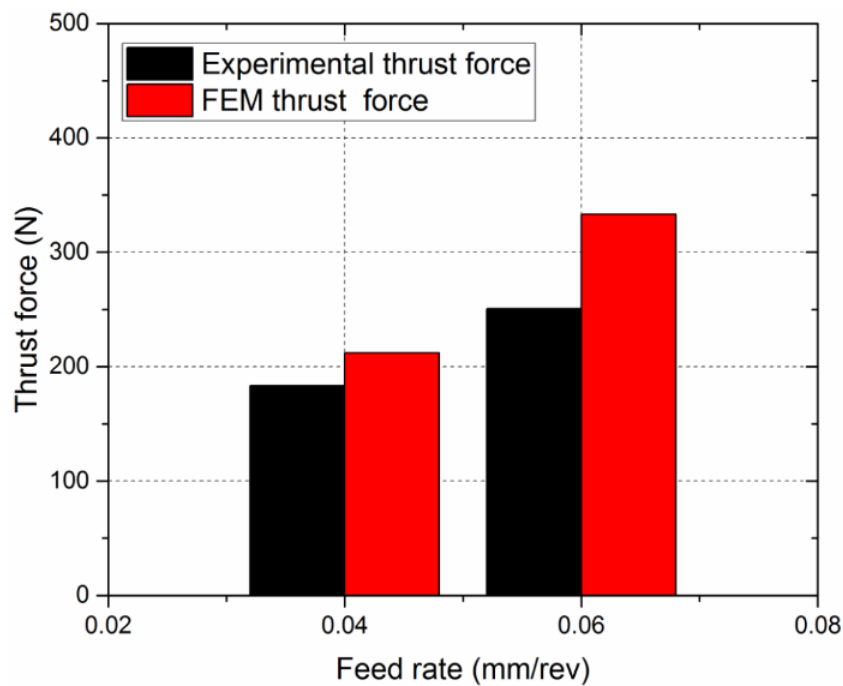
(b)

Fig. 4-7. Thrust force of Z-direction (5000rpm, 0.06mm/rev) (a) experimental result (b) simulation result

To verify the developed FE model, thrust forces of FE model and that of experiment were compared as shown in figure 4-8. In the graph of 5000rpm, error rate of FE model and experimental thrust forces was less than about 7%. In the graphs of 6000rpm and 7000rpm, error rate of the lower feed rate was lower than high. Therefore, accuracy of developed FE model was identified about 70% from those results.

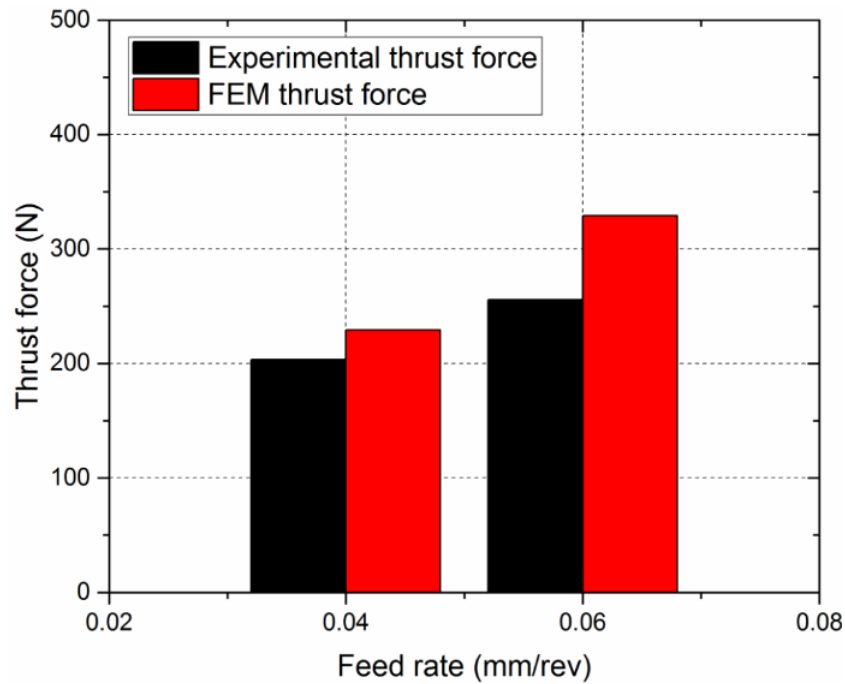


(a)



(b)





(c)

Fig. 4-8. Thrust force comparison with FE model and experiment (a) 5000rpm (b) 6000rpm (c) 7000rpm

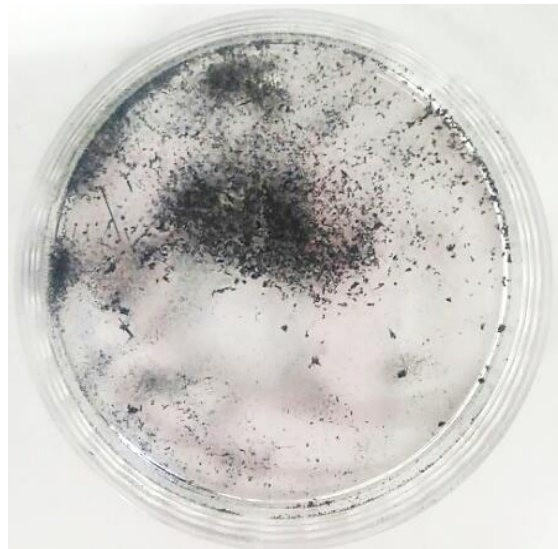
Table 4-2. Thrust force comparison of simulation and experiment

Spindle speed [rpm]	5000		6000		7000	
Feed rate [mm/rev]	0.04	0.06	0.04	0.06	0.04	0.06
Experimental thrust force [N]	202.1	215.2	183.6	250.5	203.3	255.8
FE model thrust force [N]	252.5	259.1	211.88	333.2	229.3	329.2
Error	6.48 %	2.61 %	15.4 %	33.21 %	12.79 %	28.69 %

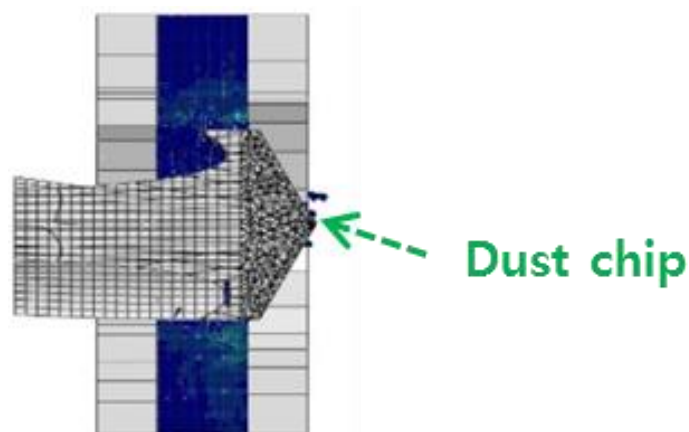


#### 4.2.2 Chip morphology

The chip morphology of experimental drilling is dust shape as figure 4-9 shows. Also, the chip shape in FE model was dust chip as figure 4-9 (b) shows. The chip morphology of CFRP drilling was related to fiber orientation. It is related with the composite machining mechanism of SEM image in figure 4-10. When the fiber orientation is lesser than  $90^\circ$ , fiber section of CFRP chip was well-cut. In the contrast, the fiber orientation is greater than  $90^\circ$ , fiber section of chip morphology was crumpled and torn shapes. In this experiment, various chip morphologies were identified in the figure 4-10 showing well-cut shapes (figure 4-10 (a)) and crumpled, torn (figure 4-10 (b)) . This is because the drill bit were cutting various fiber orientations with the rotational motion of the drill bit.

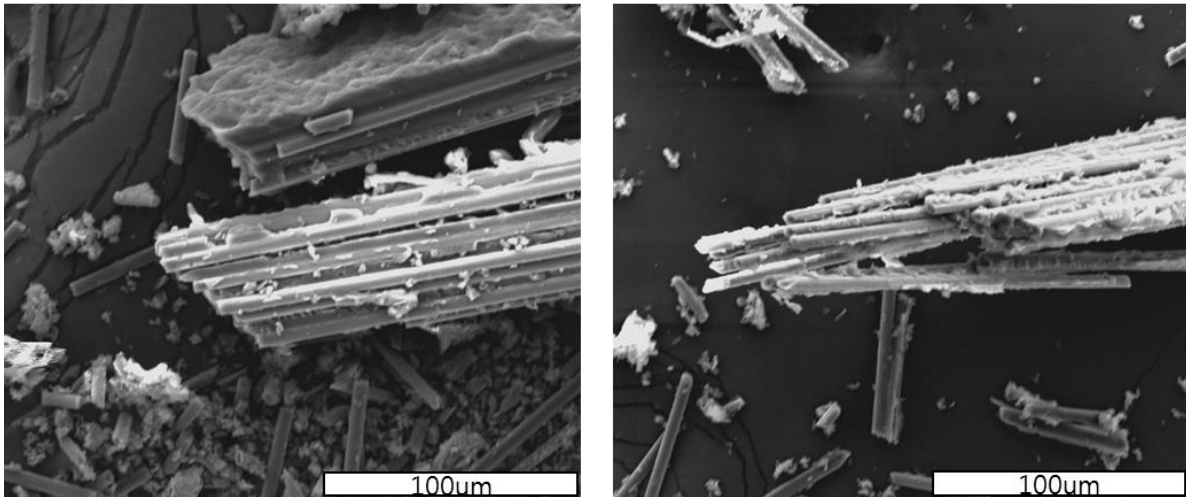


(a)

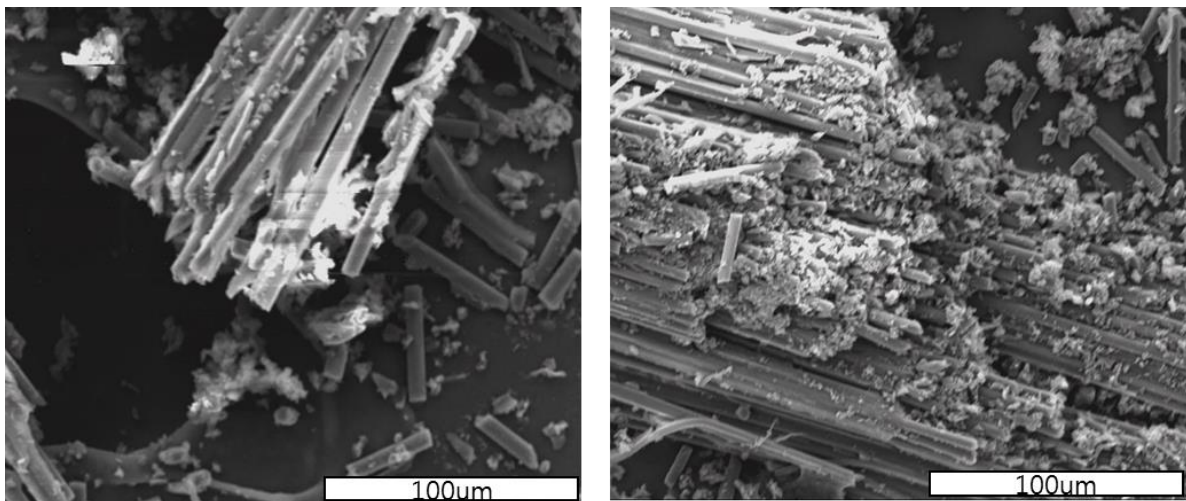


(b)

Fig. 4-9. Chip morphology (a) experimental chip (b) FE model chip



(a)



(b)

Fig. 4-10. SEM image of CFRP chip morphology  
 (a) fiber orientation  $<90^\circ$  (b) fiber orientation  $>90^\circ$

### 4.2.3 Defects

There are some defects such as uncut fiber and delamination in CFRP specimens after drilling. We compared with defects of FE model and experimental results as shown in figure 4-11. The cutting condition of this picture was 5000rpm and feed rate 0.06mm/rev. Figure 4-11 shows the uncut fibers, the machinability at the outlet section, and hence, we can state that defects of FE model and those of experiment are similar to each other.

The machinability of drilling process is shown in figure 4-12. In this figure, the hole quality with a cutting condition of 7000rpm showed better outlook than that of other cutting conditions. Also, machinability of lower feed rate was better than high in the same spindle speed.

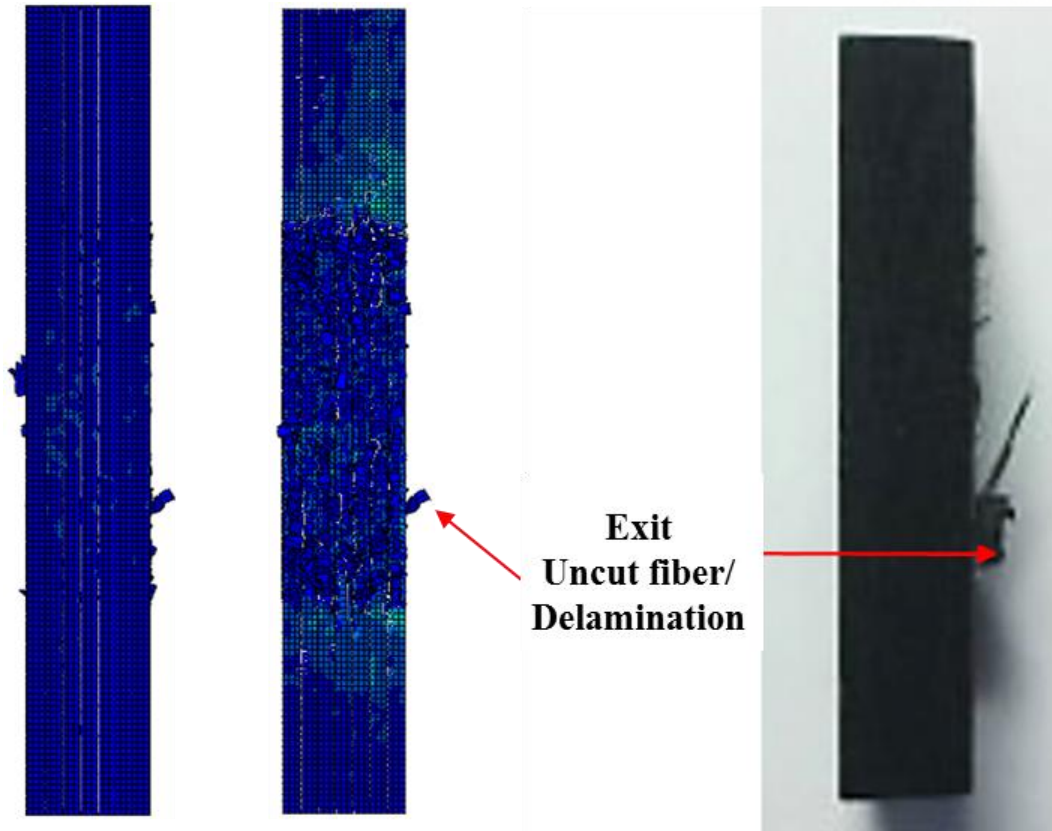


Fig. 4-11. Defects comparison of FE model and experimental result after drilling process  
(5000rpm, 0.06mm/rev)







Spindle speed Feed rate	5000rpm	6000rpm	7000rpm
0.04 mm/rev			
0.06 mm/rev			

Fig. 4-12. Comparison of CFRP specimens between FE model and experimental results

### 4.3 Summary

This chapter consists of result description and deep investigation of the FE model and that of the experiments. Functions represented in chapter 3 as well as the theories introduced in chapter 2 were applied to the simulation. Thrust force was predicted using ABAQUS with same loading conditions of the experiments. Besides, defect such as the uncut fiber was predicted by simulation. During the experiments, thrust force was measured by the dynamometer, and they were, consequently, utilized for the simulation analysis validation.

## 5. CONCLUSIONS AND FUTURE WORK

### 5.1 Contributions and Conclusions

The aim of this research is to develop the FE model to foresee the defects and cutting force during CFRP drilling. This thesis presents the simplified FE model and the method to predict mechanical phenomenon during drilling process. FE model of CFRP drilling was developed by commercial software ABAQUS.

The characteristics of the CFRP machining and the methods for the analysis were presented in the literature review. CFRP machining is distinguished from traditional metal cutting since a CFRP demonstrates heterogeneous characteristics. For example, fiber orientation affects the chip morphology in CFRP cutting. Plus, thrust force in CFRP drilling process is another important factor causing delamination.

In chapter 3, the analysis model of CFRP drilling was developed. Damage, delamination, and boundary condition modeling were considered for the simulation using VUMAT. Damage model is adapted with Hashin criteria in the fiber failure and Puck criteria in the matrix failure. In addition, delamination modeling was applied using cohesive zone. Moreover, friction test was performed by pin-on-disc test to investigate the friction coefficient. Pin material used in this test was same with drill bit. Friction coefficient was applying for the analysis of FE model of CFRP drilling.

In chapter 4, CFRP drilling simulation consisted using the method and conditions presented in previous chapter. Thrust force of developed FE model shows the change of the thrust force according to the drill entry position at the time of drilling was confirmed. Simulation results compared with the experimental results to investigate an accuracy of developed FE model. The result error of thrust force was about 7% to 33% in FE model results. In addition, chip morphology and uncut fiber shown in the FE model were almost same with experimental results.

Developed FE model can predict the delamination which related to the stress distribution occurring in each layer. In addition, they are available to suggest optimum cutting condition.

## 5.2 Future work

Developed FE model applied for simplification 3D drill model. Those factor caused simulation not to be correctly matched to the experiment in terms of thrust force. In the future research, it is imperative to check the error rate of thrust force between the experiment and the analysis by considering the complex section to the 3D drill model. Maximum error rate of thrust force between the experimental and simulation results will be available to reduce to less than 20% for increase FE model accuracy. Also, FE model considers heat occurring in drilling process since it is important factor in machining. Furthermore, FE model of CFRP drilling process can be developed by applying a metal stack CFRP based on developed FE model.



## REFERENCE

- [1] Khashaba, U.A., 2004. Delamination in drilling GFR-thermoset composites. *Composite Structure*, 63, 313–327.
- [2] Abrate, S., 1997. Machining of composite materials. In: Mallick, P.K. *Composites Engineering Handbook*, 777–809.
- [3] Persson, E., Eriksson, I., Zackrisson, L., 1997. Effects of hole machining defects on strength and fatigue life of composite laminates. *Composite Part A: Applied Science and Manufacturing*, 28, 141–151.
- [4] Persson, E., Eriksson, I., Hammersberg, P. 1997. Propagation of hole machining defects in pin-loaded composite laminates. *Journal of Composite Materials*, 31, 383–408.
- [5] Hocheng, H., Dharan, C.K.H. 1990. Delamination during drilling in composite laminates. *J. Eng. Ind.* 112, 236–239.
- [6] Jain, S., Yang, D.C.H., 1993. Effects of feed-rate and chisel edge on delamination in composites drilling. *The American Society of Mechanical Engineers*, 115, 398–405.
- [7] Lachaud, F., Piquet, R., Collombet, F., Surcin, L. 2001. Drilling of composite structures. *Composite Structure*, 52, 511–516.
- [8] Pyo Jung, J., Woo Kim, G., Yong Lee, K. 2005. Critical thrust force at delamination propagation during drilling of angle-ply laminates. *Composite Structure*, 68, 391–397.
- [9] Zhang, L.B., Wang, L.J., Liu, X.Y. 2001. A mechanical model for predicting critical thrust forces in drilling composite laminates. *Proceeding of the Institution of Mechanical Engineers, Part B: Journal of Engineering Manufacture*, 215, 135–146.
- [10] Arola, D., Ramulu, M. 1997. Orthogonal cutting of fiber-reinforced composites: a finite element analysis. *International Journal of Mechanical Sciences*, 39, 597–613.
- [11] Zitoune, R., Collombet, F. 2007. Numerical prediction of the thrust force responsible of delamination during the drilling of the long-fibre composite structures. *Composite Part A:*

*Applied Science and Manufacturing*, 38, 858–866.

- [12] Zitoune, R., Collombet, F., Lachaud, F., Piquet, R., Pasquet, P. 2005. Experiment-calculation comparison of the cutting conditions representative of the long fiber composite drilling phase. *Composite Science and Technology*, 65, 455–466.
- [13] Durão, L.M.P., de Moura, M.F.S.F., Marques, A.T. 2006. Numerical simulation of the drilling process on carbon/epoxy composite laminates. *Composite Part A: Applied Science and Manufacturing*, 37, 1325–1333.
- [14] Durão, L.M.P., de Moura, M.F.S.F., Marques, A.T. 2008. Numerical prediction of delamination onset in carbon/epoxy composites drilling. *Eng. Fract. Mech.* 75, 2767–2778.
- [15] Jamal Y. Sheikh-Ahmad, 2009. Machining of polymer composites.
- [16] Famal Y. Sheikh-Ahmad, Machining of Polymer composites.
- [17] Kobayashi, A., Robert E. Kreiger, Malabar, FL, 1981. Machining of Plastics.
- [18] Wang D. H., M. Ramulu M. and Arola D. 1995. Orthogonal cutting mechanisms of graphite/epoxy composite. Part1: Unidirectional laminate. *International Journal of Machine Tools and Manufacture*, 35, pp. 1639-1648.
- [19] Sheikh-Ahmad J. Y. 2009. Machining of Polymer Composites, New York: Springer.
- [20] Calzada K. A. 2012. Modeling and interpretation of fiber orientation-based failure mechanisms in machining of carbon fiber-reinforced polymer composites. *Journal of Manufacturing Processes*, 14, 141-149.
- [21] Ramulu M. 1997. Machining and surface integrity of fibre-reinforced plastic composites. *Sadhana*, vol. 22, 449-472.
- [22] Wang D. H., Ramulu M. and Arola D. 1995. Orthogonal cutting mechanisms of graphite/epoxy composite. Part II: multi-directional laminate," *International Journal of Machine Tools and Manufacture*, vol. 35, no. 12, pp. 1639-1648, 12 1995.
- [23] Zitoune R., Collombet R. and Lachaud F. 2005. Experiment–calculation comparison of the cutting conditions representative of the long fiber composite drilling phase. *Composites Science and Technology*, 65, 455-466.



- [24] Venu Gopala Rao G., Mahajan P. and Bhatnagar N. 2008. Three-dimensional macromechanical finite element model for machining of unidirectional-fiber reinforced polymer composites. *Materials Science and Engineering: A*, 498, 142-149.
- [25] Mkaddem A. and El Mansori M. 2009. Finite element analysis when machining UGFreinforced PMCs plates: Chip formation, crack propagation and induced-damage. *Materials & Design*, 30,3295-3302.
- [26] Iliescu D., Gehin D., Iordanoff I., Girot F. and Gutierrez M. 2010. A discrete element method for the simulation of CFRP cutting. *Composites Science and Technology*, 70, 73-80.
- [27] Santiuste C., Soldani X. and Miguelez M. H. 2010. Machining FEM model of long fiber composites for aeronautical components. *Composite Structures*, 92, 691-698.
- [28] Mackerle J. 1998. Finite-element analysis and simulation of machining: a bibliography (1976-1996). *Journal of Materials Processing Technology*, 89, 17-44.
- [29] Mackerle J. 2003. Finite-element analysis and simulation of machining: an addendum: A bibliography (1996-2002). *International Journal of Machine Tools and Manufacture*, 43,103-114.
- [30] Lasri L., Nouari M. and El Mansori M. 2009. Modelling of chip separation in machining unidirectional FRP composites by stiffness degradation concept. *Composites Science and Technology*, 69, 684-692.
- [31] Venu Gopala Rao G., Mahajan P. and Bhatnagar N. 2007. Micro-mechanical modeling of machining of FRP composites- Cutting force analysis. *Composites Science and Technology*, 67, 579-593.
- [32] Venu Gopala Rao G., P. Mahajan and N. Bhatnagar, 2007. Machining of UD-GFRP composites chip formation mechanism. *composites Science and Technology*, 67, 2271-2281.
- [33] Venu Gopala Rao G., Mahajan P. and Bhatnagar N. 2008. Three-dimensional macro-mechanical finite element model for machining of unidirectional-fiber reinforced polymer composites. *Materials Science and Engineering: A*, 498, 142-149.
- [34] Mkaddem A. and El Mansori M. 2009. Finite element analysis when machining UGF-

reinforced PMCs plates: Chip formation, crack propagation and induced-damage. *Materials & Design*, 30, 3295-3302.

- [35] Iliescu D., Gehin D., Iordanoff I., Girot F. and Gutierrez M. 2010. A discrete element method for the simulation of CFRP cutting. *Composites Science and Technology*, 70, 73-80..
- [36] Rentsch R., Pecat O. and Brinksmeier E. 2011. Macro and micro process modeling of the cutting of carbon fiber reinforced plastics using FEM. *Procedia Engineering*, 10, 1823-1828.
- [37] Rentsch R., Pecat O. and Brinksmeier E. 2011. Macro and micro process modeling of the cutting of carbon fiber reinforced plastics using FEM. *Procedia Engineering*, 10, 1823-1828.
- [38] U.S. Department of Transportation - Federal Aviation Administration, 1996. Comparative Evaluation of Failure Analysis Methods for Composites Laminates. *Office of Aviation Research, Washington*.
- [39] Mohite P. 2009. Hashin Failure Criteria for Unidirectional Fiber Composites. *Department of Aerospace Engineering, Kanpur*.
- [40] Feraboli P., Wade B., Deleo F., Rassaian M., Higgins M. and Byar A. 2011. LS-DYNA MAT54 modeling of the axial crushing of a composite tape sinusoidal specimen. *Composites Part A: Applied Science and Manufacturing*, 42, 1809-1825.
- [41] Norman J., Knight F. 2006. User-Defined Material Model for Progressive Failure Analysis. *NASA, Hampton*.
- [42] Mohite P., 2009. Hashin Failure Criteria for Unidirectional Fiber Composites. *Department of Aerospace Engineering, Kanpur*.
- [43] Nayak D., Singh I., Bhatnagar N. and Mahajan P. 2004. An analysis of machining induced damages in FRP Composites – A micromechanics Finite Element Approach. *Materials Processing and Design: Modeling, Simulation and Applications*, 712, 327-331.
- [44] Vaibhav A. Phadnis, Farrukh Makhdum, Anish Roy, Vadim V. Silberschmidt, 2013. Drilling in carbon/epoxy composites: experimental investigations and finite element implementation. *Composites: Part A*, 47, 41–51.
- [45] Feito N., López-Puente J., Santiuste C., Miguélez M.H. 2014. Numerical prediction of

delamination in CFRP drilling. *Composite structures*, 108, 677–683.

- [46] Feito N., Diaz-Álvarez J., López-Puente J., Miguelez M.H. 2016. Numerical analysis of the influence of tool wear and special cutting geometry when drilling woven CFRPs. *Composite Structures*, 138, 285–294.
- [47] Hibbitt, Karlsson & Sorenwen Inc., 2011, ABAQUS version 6.11
- [48] Jinqang Xu, Mohamed El Mansori, 2016, Numerical modeling of stacked composite CFRP/Ti machining under different cutting sequence strategies. *International journal of precision engineering and manufacturing*, 17, 99-107.
- [49] Dandekar C. R., Shin Y. C. 2012, Modeling of machining of composite materials; a review. *International Journal of machine Tool Manufacture*, 57, 102-121.
- [50] Hinton M. J., Kaddour A. S., Soden P. D. 2002. A comparison of the predictive capabilities of current failure theories for composite laminates, judged against experimental evidence. *Compos Science Technology*, 62, 1725-1797.
- [51] Vaibhav A. Phadnis, Farrukh Makhdum, Anish Roy, Vadim V. Silberschmidt, 2013. Drilling in carbon/epoxy composites: Experimental investigations and finite element implementation. *Composites: Part A*, 47, 41-51.
- [52] Hou J. P., Oetrubuc B., Ryuz C., Gakkett S. R. 2000. Prediction of impact damage in composite plates. *Composite science*, 60, 273-281.
- [53] Fish J. C., Lee S. W. 1989. Delamination of tapered composite structures. *Engineering Fracture Mechanics*, 34, 43-54.
- [54] Hibbitt, Karlsson & Sorenwen Inc. 2014. Abaqus version 6.14

## ACKNOWLEDGEMENTS

First of all, I would like to express my sincerest appreciation to my advisor professor Hyung Wook Park. Thanks to his kind and considerate guidance and knowledge, this research was successfully completed. I was so honored to be able to study under professor Hyung Wook Park.

Also, I would like to express my sincere gratitude to committee members, professor Young-Bin Park and Namhun Kim. Thanks to their informative advice, this research was successfully completed.

I am really grateful to lab members in Multi-scale Hybrid Manufacturing Laboratory; Dr. Deka, Dr. Hazarika, Dr. Nilanjan, Dr. Kyoung Il Kong, Dr. Dong Min Kim, Ji Su Kim, Jae Woo Seo, Do Young Kim, O Bum Kwon, Young Bin Kim, Wu Jin Lee and Yeon Oh Kim for their support.

Especially, I would like to thank Dr. Nilanjan, Dr. Dong Min Kim, Young Bin Kim and Do Young Kim. They gave me lots of advices and helps for my study. With their warm kindness and help, I could finish my study successfully.

I would sincerely like to express my deep appreciation to my family for their constant support and trust. My parents and brother were strong and supportive to me. They gave me unceasing courage and hope. I will be a proud daughter and sister to my family.

Last but not least, I would like to say thank you to all those who did not mention it.

Thanks.